Published in final edited form as:

Nature. 2019 October ; 574(7780): 696–701. doi:10.1038/s41586-019-1671-8.

MHC-II neoantigens shape tumor immunity and response to immunotherapy

Elise Alspach[1,2], **Danielle M. Lussier**[1,2], **Alexander P. Miceli**[1,2], **Ilya Kizhvatov**[1], **Michel DuPage**[5,#], **Adrienne M. Luoma**[4], **Wei Meng**[1,2], **Cheryl F. Lichti**[1,2], **Ekaterina Esaulova**[1], **Anthony N. Vomund**[1], **Daniele Runci**[1,2], **Jeffrey P. Ward**[1,2,3], **Matthew M. Gubin**[1,2], **Ruan F.V. Medrano**[1,2], **Cora D. Arthur**[1,2], **J. Michael White**[1], **Kathleen C.F. Sheehan**[1,2], **Alex Chen**[1], **Kai W. Wucherpfennig**[4], **Tyler Jacks**[5,6], **Emil R. Unanue**[1], **Maxim N. Artyomov**[1], **Robert D. Schreiber**[1,2,*]

[1]Department of Pathology and Immunology, Washington University School of Medicine

[2]The Andrew M. and Jane M. Bursky Center for Human Immunology and Immunotherapy Programs, Washington University School of Medicine

[3]Division of Oncology, Department of Medicine, Washington University School of Medicine

[4]Department of Cancer Immunology and Virology, Dana-Farber Cancer Institute

[*]Correspondence and requests for materials should be addressed to rdschreiber@wustl.edu.
[#]Current address: Division of Immunology and Pathogenesis, Department of Molecular and Cell Biology, University of California Berkeley, Berkeley, CA, USA.

AUTHOR CONTRIBUTIONS

E.A. conceived and designed the experiments, collected the data, performed and interpreted the analyses, and wrote the manuscript. D.M.L and A.P.M planned experiments, and collected and analyzed data. I.K. conceived of and designed the hmMHC algorithm and performed analyses using it, and wrote the methodological description found in this manuscript. M.D. generated the KP9025 sarcoma cell line. A.M.L provided technical assistance and helped plan experiments using MHC class II tetramers. W.M. and C.F.L. planned, performed and analyzed mass spectrometry experiments. E.E. assisted with bioinformatics analyses. A.N.V. assisted with the generation of the $CD4^+$ T cell hybridomas, and helped design and perform experiments using them. D.R. designed, collected, and analyzed data for experiments involving multi-color flow cytometry. J.P.W. provided technical support for MHC class I tetramer staining. M.M.G assisted in experiment planning. R.F.V.M. collected and analyzed data for experiments involving multi-color flow cytometry. C.D.A., K.C.F.S. and J.M.W. provided technical assistance throughout the study. A.C. collected data. K.W.W. provided mITGB1-MHC class II monomers and provided assistance in experimental design. T.J. provided support in experimental design and data analysis regarding the KP9025 sarcoma line. M.N.A. conceived and designed the hmMHC algorithm and provided bioinformatics support. E.R.U. provided assistance in experimental design. R.D.S. conceived experiments, interpreted data, and wrote the manuscript. All authors contributed to manuscript revision.

R.D.S. is a cofounder, scientific advisory board member, stockholder, and royalty recipient of Jounce Therapeutics and Neon Therapeutics and is a scientific advisory board member for A2 Biotherapeutics, BioLegend, Codiak Biosciences, Constellation Pharmaceuticals, NGM Biopharmaceuticals and Sensei Biotherapeutics. K.W.W. serves on the scientific advisory board of Tscan Therapeutics and Nextechinvest and receives sponsored research funding from Bristol-Myers Squibb and Novartis; these activities are not related to the findings described in this publication. T.J. is a member of the Board of Directors of Amgen and Thermo Fisher Scientific. He is also a co-Founder of Dragonfly Therapeutics and T2 Biosystems. T.J. serves on the Scientific Advisory Board of Dragonfly Therapeutics, SQZ Biotech, and Skyhawk Therapeutics. None of these affiliations represent a conflict of interest with respect to the design or execution of this study or interpretation of data presented in this manuscript. Dr. Jacks's laboratory currently also receives funding from the Johnson & Johnson Lung Cancer Initiative and Calico, but this funding did not support the research described in this manuscript.

DATA AVAILABILITY

Nucleotide variant calls generated from cDNA capture sequencing of the T3 and KP9025 sarcoma lines and used in the prediction of antigens shown in Figure 1a, Extended Data Figure 3a–b, and Extended Data Figure 6b are available within the article as Supplementary Data 1 and Supplementary Data 2.

CODE AVAILABILITY

Code for the hmMHC algorithm used to predict presentation of neoantigens by $I\text{-}A^b$ can be accessed at https://github.com/artyomovlab/hmmhc.

[5]David H. Koch Institute for Integrative Cancer Research, Massachusetts Institute of Technology

[6]Howard Hughes Medical Institute, Massachusetts Institute of Technology

Abstract

The ability of the immune system to eliminate and shape the immunogenicity of tumors defines the process of cancer immunoediting[1]. Immunotherapies such as those that target immune checkpoint molecules can be used to augment immune-mediated elimination of tumors and have resulted in durable responses in cancer patients that did not respond to previous treatments. However, only a subset of patients benefit from immunotherapy and more knowledge about what is required for successful treatment is needed[2–4]. While the role of tumor neoantigen-specific $CD8^+$ T cells in tumor rejection is well established[5–9], the roles played by other T cell subsets have received less attention. Here we show spontaneous and immunotherapy-induced anti-tumor responses require the activity of both tumor antigen specific $CD8^+$ and $CD4^+$ T cells, even in tumors that do not express MHC class II. Additionally, tumor cell expression of MHC class II-restricted antigens is required at the site of successful rejection, indicating that $CD4^+$ T cell activation must also occur in the tumor microenvironment. These findings suggest that MHC class II-restricted neoantigens have a key function in the anti-tumor response that is nonoverlapping with that of MHC class I-restricted neoantigens and therefore need to be considered when identifying patients who will most benefit from immunotherapy.

Immune checkpoint therapy (ICT) demonstrates remarkable clinical efficacy in subsets of cancer patients but many fail to develop durable responses[2–4]. Although MHC class I (MHC-I)-restricted neoantigens are important targets of tumor-specific $CD8^+$ cytotoxic T lymphocytes (CTL) during successful ICT in both mice and humans[5–12], current methods to predict patient response to ICT are imprecise and additional or better prognostic indicators are needed[13–17]. The influence of MHC class II (MHC-II)-restricted $CD4^+$ T cell responses to tumor neoantigens during immunotherapy has only recently been addressed[18,19]. While some reports show that effective tumor immunity can occur in the absence of $CD4^+$ T cell help, most indicate that $CD4^+$ T cells play important roles in generating tumor-specific $CD8^+$ T cells[20–25]. However, since it has proven difficult to identify tumor-specific mutations that function as neoantigens for $CD4^+$ T cells using existing MHC-II antigen prediction algorithms, considerable uncertainty remains as to whether strict tumor specificity in the $CD4^+$ T cell compartment is required during spontaneous or ICT-induced anti-tumor responses[26,24,27] especially for tumors that do not express MHC-II.

Herein we use the well characterized, MHC-II-negative T3 methylcholanthrene (MCA)-induced sarcoma line that grows progressively in wild-type (WT) mice but is rejected following ICT in a $CD4^+$ and $CD8^+$ T cell dependent manner[9]. Although we have identified point mutations in laminin-α subunit 4 (G1254VLAMA4; mLAMA4) and asparagine-linked glycosylation 8 glucosyltransferase (A506TALG8; mALG8) as major MHC-I neoantigens in T3, the identities of T3-specific MHC-II antigens remain unknown[9]. Using newly developed predictive algorithms, we identify an N710Y somatic point mutation in integrin-β1 (mITGB1) as a major MHC-II neoantigen of T3 sarcoma cells. Employing nonimmunogenic oncogene-driven sarcoma cells (KP9025) that lack mutational neoantigens, we demonstrate

that co-expression of single MHC-I and MHC-II T3 neoantigens renders KP9025 cells susceptible to ICT. We find similar requirements for vaccines that drive rejection of T3 tumors. In mice bearing contralateral KP.mLAMA4.mITGB1 and KP.mLAMA4 tumors, ICT induces rejection of tumors expressing both neoantigens but not tumors expressing mLAMA4 only, indicating that co-expression of both MHC-I and MHC-II neoantigens at the tumor site is necessary for successful ICT. These results show that expression of MHC-II neoantigens in tumors is a critical determinant of responsiveness to ICT, personalized cancer vaccines and potentially other immunotherapies.

Predicting MHC-II neoantigens with hmMHC

The best currently available methods for predicting MHC-II restricted neoantigens rely on tools (netMHCII-2.3 and netMHCIIpan-3.2) that are inaccurate partially due to the open structure of the MHC-II binding groove leading to significant epitope length variability[18,26]. Moreover, the existing tools cannot be re-trained on new data. We therefore developed a hidden Markov model-based MHC binding predictor (hmMHC, Extended Data Fig. 1a) that inherently accommodates peptide sequences of variable length and is trained on recent Immune Epitope Database (IEDB) content (Extended Data Fig. 1b–d). Validation analyses showed hmMHC to be superior to other predictors since it displays substantially higher sensitivity for high specificity values (Extended Data Figure 2a–b). Using hmMHC, we calculated the likelihood of each of the 700 missense mutations expressed in T3 (Supplementary Data 1) being presented by I-A^b and refined our results by prioritizing candidates based on I-A^b binding affinity, mutant:wild type I-A^b binding ratios, and transcript abundance (Fig. 1a, Extended Data Fig. 3a)[18].

One candidate, an N710Y mutant of integrin β1 (mITGB1), met all our criteria (Fig. 1a, Extended Data Fig. 3a). Notably, mITGB1 was not selected using netMHCII-2.3 or netMHCIIpan-3.2 (Extended Data Fig. 3b, data not shown). ELISPOT analysis showed that the mITGB1 peptide induced high IFNγ production from $CD4^+$ T3 tumor infiltrating lymphocytes (TIL). Other mutant peptides that fulfilled some but not all of our criteria induced only weak or absent responses, thereby validating our hmMHC prediction method (Fig. 1b, Extended Data Fig. 3c, Supplemental Table 1). To confirm this result, T3-derived $CD4^+$ TIL were stained with MHC-II tetramers carrying either the 707-721 mITGB1 peptide or irrelevant peptide (CLIP). Whereas 5.9% of T3-infiltrating $CD4^+$ T cells stained positively with the mITGB1-I-A^b tetramer, the CLIP-I-A^b tetramer stained only 0.7% of the cells (Fig. 1c, Extended Data Fig. 3d–e). Cytokine profiling of mITGB1-specific $CD4^+$ TIL from T3 tumors revealed that they produced IFNγ, TNFα, and IL-2 but not IL-4, IL-10, IL-17 or IL-22, indicating a Th1-like phenotype (Extended Data Fig. 3f). T3-bearing mice treated with ICT did not develop additional MHC-II neoantigen specificities (data not shown). To assess whether T3-specific $CD4^+$ T cells selectively recognized the mutant, we compared mutant to WT Itgb1 peptides in ELISPOT analyses using freshly isolated T3 $CD4^+$ TIL. Positive responses were seen only with mITGB1 peptide (Fig. 1d). Similar data were obtained using $CD4^+$ T cell hybridomas generated from T3 TIL (Extended Data Fig. 4, Extended Data Fig. 5a).

Mapping experiments revealed that the MHC-II binding core of mITGB1 consists of 9 amino acids (^{710}YNEAIVHVV^{718}) where the mutant Y710 residue functions as an I-A^b anchor (Extended Data Fig. 5b). To verify that the mITGB1 epitope is physiologically presented by MHC-II, T3 cells were transduced with a vector encoding the mouse MHC-II transactivator CIITA (T3.CIITA) that induced high levels of I-A^b expression (Extended Data Fig. 5c)[28]. Elution of peptides bound to I-A^b on T3.CIITA and analysis by mass spectrometry identified two mITGB1 peptides encompassing the Y710 mutation (a 17mer and a 14mer; Fig. 1e, Extended Data Fig. 5d). Peptides with the corresponding WT sequence were not found. The mITGB1 epitope was also not detected in MHC-I eluates from IFNγ-stimulated T3 cells, and mITGB1-specific CD8$^+$ T cells were not observed by cytokine production (data not shown). Together, these data demonstrate that mITGB1 is a major MHC-II-restricted neoantigen of T3 sarcoma cells.

ICT response requires CD4$^+$ T cell help

Recent publications highlight the ability of CD4$^+$ T cells to recognize tumor-specific antigens and promote tumor rejection in the absence of ICT[18,29,30]. To assess whether CD4$^+$ T cells are required during ICT-induced rejection, we expressed MHC-I and/or MHC-II neoantigens from T3 sarcoma cells in an oncogene-driven sarcoma cell line generated from a Kras$^{LSL\text{-}G12D/+}$ x p53$^{fl/fl}$ mouse injected intramuscularly with lentiviral cre-recombinase (KP9025)[7]. The unmodified KP9025 sarcoma line formed progressively growing tumors in either syngeneic WT mice treated with or without dual anti-PD-1/anti-CTLA4 ICT or mice rechallenged with unmodified KP9025 after previously being cured of their KP9025 tumors via surgical resection (Fig. 2a–b). As this challenge-resection-rechallenge approach promotes immune control or rejection of even poorly immunogenic tumor cells used in the initial priming step[31], these results supported the conclusion that KP9025 sarcoma cells were not immunogenic. Whole exome sequencing revealed that KP9025 cells expressed only 4 nonsynonymous mutations (Supplementary Data 2) and none were predicted to be immunogenic (Extended Data Fig. 6a–b, Supplemental Table 2). Enforced expression of either mLAMA4 or mITGB1 alone did not render KP9025 cells immunogenic in WT mice in the presence or absence of ICT (Fig. 2c, Extended Data Fig. 6d–e). Progressively growing KP.mLAMA4 tumors maintained expression of their MHC-I tumor neoantigen, thereby ruling out antigen loss via immunoediting (Extended Data Fig. 7a). KP9025 cells expressing both mLAMA4 and mITGB1 formed tumors in immunodeficient *Rag2*$^{-/-}$ mice that grew with kinetics similar to KP.mLAMA4 or KP.mITGB1 cells (Extended Data Fig. 6c). However, growth of KP.mLAMA4.mITGB1 cells in WT mice treated with control mAb was noticeably slower than that of either single-antigen expressing cell line and KP.mLAMA4.mITGB1 tumors were rejected in WT mice following either dual or single agent ICT despite the absence of tumor cell MHC-II expression (Fig. 2c, Extended Data Fig. 6d–e, data not shown).

We considered the possibility that the enhanced immunogenicity of KP.mLAMA4.mITGB1 tumors was merely a function of antigen quantity. Therefore, we generated KP9025 cells that lacked MHC-II neoantigens but co-expressed two strong MHC-I neoantigens: the MHC-I epitope of ovalbumin (SIINFEKL) and the R913L mutant of spectrin-β2 (mSB2), which we previously showed contributed to the spontaneous rejection of the MCA-induced d42m1

sarcoma line in WT mice[6]. KP.mSB2.SIINFEKL tumors grew progressively in mice treated either with control mAb or dual ICT, and the expression of both MHC-I antigens was maintained in growing tumors from ICT-treated animals (Fig. 2c, Extended Data Fig. 7b–d). Enforced expression of mITGB1 in KP.mSB2.SIINFEKL led to significantly increased survival of ICT-treated mice injected with the un-cloned tumor line (Extended Data Fig. 7e). Thus, tumor rejection and ICT sensitivity are dependent on combinatorial effects of $CD4^+$ and $CD8^+$ T cells.

mITGB1 $CD4^+$ T cells are Th1 polarized

We then asked whether mITGB1-specific $CD4^+$ TIL displayed a Th1 phenotype similar to that seen with T3 tumors. Seventy-four percent of mITGB1 tetramer-positive $CD4^+$ T cells in KP.mLAMA4.mITGB1 tumors from control-treated mice expressed the Th1-associated transcription factor T-BET but not the Treg-associated transcription factor FOXP3. An additional 17% expressed both T-BET and FOXP3. Conversely, tetramer-negative $CD4^+$ T cells showed substantially diminished T-BET expression (24%) and much higher FOXP3 expression (61%). mITGB1-$tetramer^+$ $CD4^+$ T cells displayed a higher $T\text{-}BET^+$:$FOXP3^+$ ratio than tetramer-negative cells (4 vs. 0.4, respectively) and this ratio was further increased in response to anti-CTLA4 treatment (33 vs. 3.7, respectively) (Extended Data Fig. 8a–c). On average, 83% of mITGB1-specific $CD4^+$ T cells expressed high levels of PD-1 compared to only 19% of mITGB1-tetramer-negative cells (Extended Data Fig. 8d–e). $CD4^+$ T cells specific for mITGB1 also expressed high levels of CD44, ICOS and CD150/SLAM, and low levels of KLRG1 (Extended Data Fig. 8f). The presence of an expanded population of Th1-like $ICOS^+$ $CD4^+$ T cells was recently reported in B16- and MC38 tumor-bearing mice treated with anti-CTLA4, although the tumor antigen specificity of this population was not identified[32]. These data, together with the cytokine profiles described above, indicate that mITGB1-specific $CD4^+$ T cells display an activated Th1 phenotype.

CTL generation requires $CD4^+$ T cell help

To identify the mechanism by which tumor neoantigen-specific $CD4^+$ T cells influence ICT-mediated anti-tumor responses, we assessed effects on $CD8^+$ T cell priming by comparing MHC-I tetramer staining of splenic mLAMA4-specific $CD8^+$ T cells from KP.mLAMA4- or KP.mLAMA4.mITGB1-bearing mice treated with control mAb or ICT. In the absence of ICT, mLAMA4-H-$2K^b$ tetramers stained only 1.2% of $CD8^+$ T cells from KP.LAMA4-bearing mice, but staining increased to 5.3% in mice bearing KP.mLAMA4.mITGB1 tumors (Fig. 3a–b). This staining pattern was unchanged in the presence of PD-1 blockade, but was increased with anti-CTLA4 treatment, either as monotherapy or in combination with anti-PD-1. This result is consistent with the observation that anti-CTLA4 functions largely to enhance $CD4^+$ T cell responses[32,33].

To assess whether MHC-II neoantigens also enhanced CTL formation, we employed an *in vivo* T cell cytotoxicity assay that monitored the capacity of naturally arising CTL to kill CFSE-labeled, peptide-pulsed splenocytes[34]. Non-tumor-bearing control mice and mice bearing KP.mLAMA4 tumors were largely incapable of eliminating mLAMA4 peptide-pulsed splenocytes either in the presence or absence of ICT (Fig. 3c, top and middle panels).

In contrast, mice bearing KP.mLAMA4.mITGB1 tumors efficiently eliminated $CFSE^{hi}$-labeled, mLAMA4 peptide-pulsed splenocytes but not $CFSE^{lo}$-labeled SIINFEKL-pulsed splenocytes and the degree of elimination of the former was enhanced by ICT (Fig. 3c, bottom panels, Fig. 3d). The cytotoxic activity of control-treated mLAMA4-specific $CD8^+$ T cells observed in the splenocyte killing assay was higher than would be expected from our *in vivo* tumor rejection experiments (Fig. 2e). This difference can most likely be explained by differences in susceptibility of splenocytes to T cell-mediated killing compared to tumor cells. Thus, $CD4^+$ T cell help enhances both $CD8^+$ T cell priming and maturation of $CD8^+$ T cells into CTL.

Vaccines require MHC-I and -II antigens

Since $CD4^+$ T cell help was critically important in generating mLAMA4-specific CTL during ICT, we tested whether mITGB1-specific $CD4^+$ T cells were also important for vaccine-elicited anti-tumor responses (Fig. 4a). Vaccination of naïve recipients with irradiated parental KP9025, KP.mLAMA4, or KP.mITGB1 cells was not sufficient to protect mice from subsequent challenge with T3 sarcoma cells. Vaccination with a mixture of irradiated KP.mLAMA4 and KP.mITGB1 cells provided protection against T3 challenge in 30% of mice. In contrast, vaccination with irradiated KP.mLAMA4.mITGB1 cells prevented T3 tumor outgrowth in 11 of 13 recipients (Fig. 4b–c). Furthermore, spleens from mice vaccinated with irradiated KP.mLAMA4.mITGB1 cells contained significantly more mLAMA4-specific, IFNγ-producing $CD8^+$ T cells compared to mice vaccinated with KP cells expressing only mLAMA4 (Fig. 4d). The differences in efficacy between mixed cellular vaccines and dual antigen-expressing KP.mLAMA4.mITGB1 vaccines support the findings by others that effective vaccines are those where the MHC-I and MHC-II epitopes reside on the same peptide strand, potentially leading to more efficient uptake and presentation of both antigens by the same antigen-presenting cell (APC)[20,35]. A similar situation would be expected to occur when both antigens were present in the same tumor cell used for vaccination.

MHC-II antigen expression at tumor site

To investigate a requirement for $CD4^+$ T cells beyond priming and maturation of anti-tumor CTL, we asked whether tumor cell expression of MHC-II neoantigens was necessary at the site of tumor rejection. We assessed *in vivo* growth of contralaterally injected KP.mLAMA4.mITGB1 and KP.mLAMA4 tumors in either immunodeficient or immunocompetent mice treated with ICT. The contralateral tumors grew at equivalent rates in *Rag2*$^{-/-}$ mice (Extended Data Fig. 9a). However, ICT treatment of WT mice bearing contralateral tumors resulted in complete rejection of the KP.mLAMA4.mITGB1 tumor but only delayed outgrowth of the KP.mLAMA4 tumor on the opposite flank (Fig. 5a–b). This result shows that CTL specific for mLAMA4 can control tumors expressing both the cognate MHC-I epitope and the helper MHC-II epitope locally but function poorly against distant yet related tumors lacking CD4 neoepitopes. In similar experiments, we asked if mITGB1-specific $CD4^+$ T cells generated from KP.mLAMA4.mITGB1 tumors were sufficient to control outgrowth of KP.mITGB1 tumors on the opposite flank. In this setting, contralateral KP.mITGB1 tumor growth was identical to that observed in mice bearing only a single

KP.mITGB1 tumor (Extended Data Fig. 9b–c). Together, these results show that tumor cell expression of MHC-II-restricted neoantigens and the presence of tumor-specific $CD4^+$ T cells in the tumor microenvironment are required to maintain tumor control during ICT but are not sufficient to mediate tumor rejection by themselves.

To expand this observation, we assessed whether $CD4^+$ T cells and MHC-II neoantigen expression in tumor cells are required to maintain functional $CD8^+$ T cell memory. When mice cured of their T3 tumors by ICT treatment were rechallenged with T3 tumor cells they rejected T3. However, if mice were depleted of $CD4^+$ T cells prior to rechallenge, they did not control T3 tumor outgrowth (Extended Data Fig. 9d). In parallel experiments, mice previously cured of KP.mLAMA4.mITGB1 tumors by surgical resection were protected against subsequent rechallenge with KP.mLAMA4.mITGB1 but were unable to prevent outgrowth of KP.mLAMA4 or KP9025 tumors (Extended Data Fig. 9e). Thus, tumor cell expression of MHC-II neoantigens and $CD4^+$ T cell help are both required for maintenance of tumor-specific immunologic memory.

Lastly, we assessed whether an MHC-II tumor neoantigen can significantly affect the local tumor microenvironment (gating strategy Extended Data Fig. 10a). We previously showed that iNOS expression is higher in macrophages populating tumors destined to reject following ICT than in macrophages from progressively growing tumors, a response induced by ICT-dependent IFNγ production[33]. $iNOS^+$ macrophages were present at 3-fold higher levels in ICT-treated KP.mLAMA4.mITGB1 tumors compared to contralateral KP.mLAMA4 tumors (Extended Data Fig. 9g–h). ELISPOT analysis of tumor-infiltrating $CD4^+$ T cells showed 5.9-fold more $IFN\gamma^+$ mITGB1-specific $CD4^+$ T cells in the KP.mLAMA4.mITGB1 tumors compared to contralateral KP.mLAMA4 tumors (Fig. 5c, Extended Data Fig. 9f). Flow cytometry analysis of the lymphoid compartment (gating strategy Extended Data Fig. 10b) revealed 3.7-fold more $CD8^+$ T cells, and 9-fold more mLAMA4-specific $CD8^+$ T cells in KP.mLAMA4.mITGB1 tumors compared to KP.mLAMA4 tumors (Fig. 5d–e). We then asked if $CD4^+$ T cells were sufficient to mediate these changes by comparing $iNOS^+$ macrophages in KP.mLAMA4.mITGB1 tumors versus contralateral KP.mITGB1 tumors and observed an 83-fold higher number of $iNOS^+$ macrophages in KP.mLAMA4.mITGB1 tumors compared to KP.mITGB1 tumors (Extended Data Fig. 9i–j). Together, these data show that MHC-II-restricted anti-tumor responses are necessary but not sufficient in ICT-sensitive tumor models to induce localized effects on the immune composition of tumors.

Discussion

Work described herein focuses on the functional role of MHC-II restricted tumor neoantigens in mediating ICT-dependent anti-tumor responses in a well-characterized mouse sarcoma model. Using a novel hidden Markov model-based tool (hmMHC), we predict and then validate that an N710Y point mutation in the integrin ITGB1 forms a major MHC-II restricted neoepitope of the T3 MCA sarcoma. It is reasonable that mITGB1 represents a major MHC-II neoantigen of T3 tumor cells because ITGB1 is the second most highly expressed mutation in T3 and the point mutation in mITGB1 generates a novel anchor residue that promotes high affinity binding to $I\text{-}A^b$. Moreover, others have proposed that

secreted tumor proteins are favored targets for $CD4^+$ T cell responses because of their easier uptake by professional APCs[36]. Localization of mITGB1 on the cell membrane would likely also facilitate efficient access by APCs, although we did not directly address this question in the current study. Importantly, we do not rule out the possibility that T3 expresses other MHC-II restricted epitopes that might be elicited by vaccination[18,19]. Nevertheless, we unequivocally demonstrate herein that mITGB1 functions as a major neoantigen of T3 during naturally occurring anti-tumor responses.

By defining authentic MHC-I and MHC-II neoantigens of T3 sarcoma cells, we have shown that, in a minimal antigen system, a single clonally expressed MHC-I neoantigen (mLAMA4) and a single clonally expressed MHC-II neoantigen (mITGB1) are necessary and sufficient to render nonimmunogenic, oncogene-driven KP9025 sarcoma cells sensitive to ICT. Using KP9025 sarcoma cells expressing different combinations of mLAMA4 and/or mITGB1, we show that $CD4^+$ T cell responses are required for optimal priming of MHC-I restricted $CD8^+$ T cells and their maturation into CTL, in either the presence or absence of ICT. We also show that optimal anti-tumor responses occur when tumor cells express both MHC-I and MHC-II neoantigens. In part, this requirement reflects the potential need for $CD4^+$ T cell responses in the tumor microenvironment and, from previous work, appears to be at least partially due to IFNγ production by tumor-specific $CD4^+$ T cells[33]. We find it of particular interest that the generation of effective tumor immunity following vaccination with tumor-specific neoantigen vaccines and ICT similarly require MHC-II neoantigens. These results provide new insights into the role of MHC-II neoantigens in natural and therapeutic immune responses to tumors. They also suggest that patients with tumors that are predicted to contain immunogenic MHC-I neoantigens or have favorable tumor mutational burdens could still be unresponsive to immunotherapies, owing to the absence of immunogenic MHC-II-restricted $CD4^+$ T cell antigens. This possibility has not been critically evaluated yet, due to the past absence of reliable MHC-II prediction algorithms. Future work is needed to test this hypothesis in cancer patients undergoing immunotherapy.

METHODS

Mice

Male wild type 129S6 (for experiments involving T3 cells) mice were purchased from Taconic Farms. Male wild type 129S4 mice (for experiments involving KP9025 cells) and 129S6 $Rag2^{-/-}$ mice were bred in our specific-pathogen free facility. All *in vivo* experiments were performed in our specific-pathogen free facility and used mice between the ages of 8 and 12 weeks. All experiments were performed in accordance with procedures approved by the AAALAC-accredited Animal Studies Committee of Washington University in St. Louis and were in compliance with all relevant ethical regulations.

Tumor transplantation

T3 MCA-induced sarcoma cells were previously generated in 129S6 wild type mice. KP sarcoma cell lines were provided by T. Jacks, and were generated following intramuscular injection of lentiviral cre-recombinase in 129S4 $Kras^{LSL\text{-}G12D/+}$ x $p53^{fl/fl}$ mice. Tumor cells were cultured in RPMI media (Hyclone) supplemented with 10% FCS (Hyclone). Cell lines

were authenticated using whole exome sequencing and verification of specific antigen expression. All cell lines used tested negative for mycoplasma contamination. For transplantation, cells were washed extensively in PBS, resuspended at a density of $13.34x10^6$ cells ml^{-1} (T3) or $6.67x10^6$ cells/mL (KP sarcomas) in PBS and then 150 μl was injected subcutaneously into the rear flanks of syngeneic recipient mice. For irradiated-tumor cell vaccines, KP.mLAMA4, KP.mITGB1 or KP.mLAMA4.mITGB1 sarcoma cells were lethally irradiated with 10Gy and 500,000 cells were injected subcutaneously into 129S6 mice. T3 challenge following vaccination occurred on the opposite flank. Following tumor transplantation, animals were randomly assigned to treatment groups. No statistical methods were used to determine group size. Tumor growth was measured by calipers and individual growth curves are represented as the average of two perpendicular diameters. Tumor measurements were performed blinded to treatment group. In accordance with our IACUC-approved protocol, maximal tumor diameter was 20 mm in one direction, and in no experiments was this limit exceeded.

Tumor rechallenge

For tumor rechallenge following surgical resection, primary tumors were allowed to grow until 10 mm in size or to the time point indicated. Following surgical removal of the established tumor, animals were rested for 30 days. Animals were then rechallenged on the opposite flank with either the same tumor line used in the primary tumor challenge or the tumor line indicated. For tumor rechallenge following ICT-mediate rejection, primary tumors were rejected following treatment with combination αPD-1+αCLTA4 ICT. After tumors were no longer apparent, animals were rested for 30 days followed by rechallenge on the opposite flank with the same tumor line used in the primary challenge or the tumor line indicated.

Epitope prediction

The identification of point mutations in T3 and KP sarcomas and the prediction of MHC class I epitopes in KP and F244 sarcomas was performed as previously described[9]. To predict neoepitopes, we applied hmMHC, our newly developed hidden Markov model (HMM) -based binding predictor, trained on the most recent Immune Epitope Database (IEDB) data. Hidden Markov models inherently accommodate inputs of variable length and have already demonstrated reasonable performance in the MHC binding affinity prediction setting[37]. Our predictor utilizes a fully connected HMM with emissions representing amino acids (see a pedagogical example in Extended Data Fig. 1A). We trained the model on a set of known binders using the Baum-Welch algorithm[38], as implemented by the GHMM library. A trained HMM returns the likelihood of a peptide to be a binder, which we represent as the −10 log odds ratio, where a smaller value indicates that a peptide has a higher likelihood to be a binder. The model that we apply in this study was trained on murine H2-I-A^b binders taken from the IEDB full MHC ligand export (downloaded on 2018-11-25, containing a total of 1072460 entries). Non-binders were not used in model training. The categorization of the data into binders and non-binders was done based on the qualitative and quantitative fields of IEDB entries: binders are peptides with IC50 ≤ 500 nM or with *Positive, Positive-High* and *Positive-Intermediate* binding quality. This data came largely from mass spectrometry assays. We validated the model using the Monte Carlo

(shuffle-split) cross-validation approach, with 10 random partitions of H2-I-A^b binders from IEDB into training and validation sets, with a relative validation set size of 0.2. Since the number of non-binders in the IEDB dataset was insufficient for validation, we used decoy sets composed of random natural peptides as non-binders. Protein-coding transcript translation sequences for *Mus musculus* were obtained from GENCODE release M19 (GENCODE project, 2018); there are 65,257 translations. For every cross-validation partition, the translations were randomly cut into fragments uniformly distributed in the interval [12,24], which generated about $1.5x10^6$ fragments. Of this set of random natural peptides, a random sample 100 times the number of binders in the validation set was taken. The 100-fold bias in the number of generated non-binders and uniform distribution of their lengths are in line with the recent works on MHC binding prediction, in particular netMHCpan-4.0[39]. We have also performed experiments with the distribution of random natural peptide lengths following the distribution of lengths on the IEDB dataset (as shown in the Extended Data Fig. 1d) and found no significant difference in results in our setting compared to uniform distribution. The rationale for the 100-fold bias is that for a sample of peptide fragments from an organism, it is commonly considered that about 1% to 2% will be binding to MHC receptors. On average, there were 4,412 binders in a training set, and 771 binders and 77,086 random natural peptides in a validation set. Classification performance of our predictor is significantly higher than the performance of the two best-known class II binding predictors[40] (netMHCII-2.3 and netMHCIIpan-3.2), as compared on our 10 validation datasets. This is due, in part, to the large amount of new mass-spec data as compared to the data on which the recent netMHCII(pan) predictors were trained (netMHCIIpan-3.2 public dataset available at http://www.cbs.dtu.dk/suppl/immunology/NetMHCIIpan-3.2/ contains 1,794 measurements for H-2-I-A^b, all qualitative, of which 431 binders and 1,363 weak and non-binders). We do not exclude the possibility that netMHCII(pan), as a method, performs better than the HMM method. As the published netMHCII(pan) tools lack re-training capability, we cannot perform the comparison of the methods and draw conclusions on netMHCII(pan) performance on new qualitative data. We determined the threshold for strong binders by calibrating the predictor to return a percentile rank against a large decoy set of random natural peptides. We utilized the approach taken by the existing neural network-based predictors, where strong binders are predictions in the 2^{nd} percentile of the empirical distribution of predictions on random natural peptides[39]. The decoy set was generated from the murine proteome in the same way as for validation and consists of about $1.5x10^6$ fragments with lengths in the interval [12,24]. Predicted neoantigens were further prioritized using the neoepitope ratio (NER). NER is the ratio between the binding predictions for the mutant and wild type peptide. Expression of each mutation is represented as fragments per kilobase of transcript per million mapped reads (FPKM) generated from cDNA capture sequencing.

Peptides

All 27-mer peptides used for neoantigen screening (Supplemental Table 1) were purchased from Peptide 2.0 and HPLC purified to >95% purity. The T3-specific mutant amino acid was placed in the center of the peptide and was flanked on both sides with 13 amino acids of wild type peptide sequence.

ELISPOT

Cells from tumors or lymph nodes were enriched for $CD4^+$ or $CD8^+$ T cells using the Miltenyi mouse $CD4^+$ or $CD8^+$ enrichment kits following manufacturer's protocols. 10,000 TIL-derived T cells or 50,000 TDLN-derived T cells were stimulated with 500,000 splenocytes isolated from naïve mice pulsed with 2μg ml^{-1} 29-mer peptide (class II) or 1μM 15-mer peptide (class I). For analysis from spleens, 500,000 cells from whole-spleen preparations were used. Cells were stimulated overnight in anti-murine IFNγ-coated ELISPOT plates (Immunospot). Plates were developed following manufacturer's protocol and spots were quantified using a CTL ImmunoSpot S6 Universal machine and Professional 6.0.0 software.

Mass Spectrometry

For isolation of $I\text{-}A^b$ bound peptides, 5 X 10^8 T3.CIITA cells were washed twice with PBS and snap frozen. MHC class II molecules were isolated by immunoaffinity purification using $I\text{-}A^b$-specific antibody Y-3P (BioXCell) coupled to cyanogen bromide-activated Sepharose 4B (GE Healthcare) following previously described protocols[41]. Peptides were eluted with 0.2% trifluoroacetic acid, cleaned by detergent removal (Pierce Detergent Removal Spin Columns, Thermo Scientific) and desalting (Pierce C-18 Spin Columns, Thermo Scientific), dried, and resuspended in 2% acetonitrile (ACN)/0.1% formic acid (20 μL). For mass spectrometry, a Dionex UltiMate 1000 system (Thermo Scientific) was coupled to an Orbitrap Fusion Lumos (Thermo Scientific) through an Easy-Spray ion source (Thermo Scientific). Peptide samples were loaded (15 μL/min, 3 min) onto a trap column (100 μm x 2 cm, 5 μm Acclaim PepMap 100 C18, 50 °C), eluted (200 nL/min) onto an Easy-Spray PepMap RSLC C18 column (2 μm, 50cm x 75 μm ID, 50 °C, Thermo Scientific) and separated with the following gradient, all % Buffer B (0.1% formic acid in ACN): 0–110 min, 2%–22%; 110–120 min, 22%–35%; 120–130 min, 35–95%; 130–150 min, isocratic at 95%; 150–151 min, 95%–2%, 151–171 min, isocratic at 2%. Spray voltage was 1900V, ion transfer tube temperature was 275°C, and RF lens was 30%. MS scans were acquired in profile mode (375–1500 Da at 120K resolution (at *m/z* 200)); centroided HCD MS/MS spectra were acquired using a Top Speed method (charge states 2–7, 3 sec cycle time, threshold 2e4, quadrupole isolation (0.7 Da), 30K resolution, collision energy 30%) with dynamic exclusion enabled (5 ppm, 60 s). Raw data files were uploaded to PEAKS X (Bioinformatics Solutions) for processing, de novo sequencing and database searching against the UniProtKB/Swiss-Prot Mouse Proteome database (downloaded 1/12/2019; 22,286 entries), appended with a truncated sequence of mITGB1 (+/− 20 amino acids from the site of mutation), with mass error tolerances of 10 ppm and 0.01 Da for parent and fragment, respectively, no enzyme specificity and methionine oxidation as a variable modification. False discovery rate (FDR) estimation was enabled, and proteins were filtered for $-10\log P \geq 0$ and one unique peptide to give 1% FDR at the peptide-spectrum match level. Peptides matching to mITGB1 were manually verified by visual inspection.

Antibodies

For immune checkpoint therapy, rat IgG2a αPD1 (RMP1-14, Leinco) and murine IgG2b αCTLA4 (9D9, Leinco Technologies) were used. Mice were injected intraperitoneally with

200μg of each antibody on 3, 6 and 9 days post tumor transplant. Antibodies used for multi-color flow cytometry were CD45 (30-F11), CD11b (M1/70), Thy1.2 (30H12), CD4 (RM4-5), CD8β (YTS156.7.7), I-E/I-A (M5/114.15.2), CD64 (X54-5/7.1), Ly6G (1A8), T-BET (4B10), CD150/SLAM (TC15-12F12.2), KLRG1 (2F1), ICOS (15F9), CD44 (IM7), PD-1 (29F.1A12), SIINFEKL-H-2-K^b (25-D1.16) (BioLegend), CD24 (M1/69), F4/80 (T45-2342) (BD Biosciences), FOXP3 (FJK-16s, eBiosciences) and iNOS (CXNFT, Invitrogen). Zombie NIR (BioLegend) was used to stain for cellular viability. The BD Cytofix/Cytoperm Plus kit (BD Biosciences) was used following manufacturer's protocol for intracellular staining of iNOS, T-BET and FOXP3.

Tetramer staining

Tetramer staining for mLAMA4-specific CD8$^+$ T cells was performed as previously described[9]. I-A^b monomers bound to CLIP or mITGB1 were a gift from K. Wucherpfennig. For staining, biotinylated pI-A^b monomers were labeled at a 4:1 molar ratio with streptavidin-APC or streptavidin-PE (Prozyme). 10x10^6 cells from whole tumor digests were stained with equal amounts of APC and PE tetramer at 20μg ml^{-1} for 2 hours at room temperature. Tetramer staining was stabilized through the use of anti-PE and anti-APC cells beads (Miltenyi), similar to previously published methods for MHC-I tetramers[42] followed by surface staining for CD11b, Thy1.2 and CD4.

Multi-cytokine assay

CD4$^+$ T cells were enriched from tumors 12 days post transplant using the Miltenyi mouse CD4$^+$ enrichment kit. 10,000 enriched CD4$^+$ T cells were stimulated in serum-free media with 500,000 splenocytes isolated from naïve mice pulsed with 2μg ml^{-1} peptide. Following a 24 hour incubation, secretion of IL-10, IL-1B, IL-2, IL-4, IL-5, IL-6, IL-22, IL-9, IL-13, IL-27, IL-23, IFNγ, IL-12 p70, GM-CSF, TNFα, IL-17A and IL-18 was measured using a flow-based ProcartaPlex Th1/Th2/Th9/Th17/Th22/Treg cytokine panel (Luminex Technologies) following manufacturer's protocol.

Plasmids

Full-length mLAMA4 and mITGB1 were cloned from T3 cDNA and full-length CIITA was cloned from 129S6 splenocytes. Gene blocks encoding SIINFEKL and the minimal epitope of mSB2 were purchased from Integrated DNA Technologies. All constructs were cloned into the BglII site of pMSCV-IRES GFP (mLAMA4, CIITA, and mSB2) or pMSCV (mITGB1 and SIINFEKL) using the Gibson Assembly method (New England Biolabs). To generate neoantigen-expressing KP sarcoma cell lines and T3.CIITA, constructs were transiently transfected into Phoenix Eco cells using Fugene (Promega). After 48 hours, viral supernatants were subsequently used for transfection of KP sarcoma line 9025 or T3. KP.mLAMA4, KP.mITGB1, KP.mLAMA4.mITGB1, KP.mSB2.SIINFEKL and T3.CIITA clones were obtained by limiting dilution.

CD4$^+$ T cell hybridomas and CTLL assay

Bulk CD4$^+$ T cells from T3 tumors were isolated 12 days post-transplant and stimulated with lethally irradiated T3.CIITA cells to establish a rapidly dividing cell line. CD4$^+$ T cells

were fused with BW5147 cells and cloned via limiting dilution. To assess antigen specificity and to map the mITGB1 MHC-II binding core, splenocytes were harvested from naïve mice and pulsed with 10μg ml^{-1} peptide unless otherwise stated. 50,000 hybridoma cells were incubated with 100,000 peptide-pulsed splenocytes overnight and culture media was collected. IL-2 production was assayed by proliferation-dependent thymidine incorporation by the IL-2 dependent CTLL-2 cell line. Data is represented as counts per million (cpm).

Measuring IFNγ production by $CD8^+$ T cell clones

Tumor cells were treated with 100 U ml^{-1} IFNγ for 48 hours before use. 100,000 CTL cells specific against mLAMA4 (74.17) or mSB2 (C3) were co-cultured with 50,000 tumor cells for 48 hours. IFNγ in supernatants was quantified using IFNγ ELISA kit (eBioscience) following manufacturer's protocol.

In vivo cytotoxicity assay

For targets, splenocytes were harvested from naïve mice, stained with either 5μM or 0.5μM CFSE ($CFSE^{hi}$ and $CFSE^{lo}$) (Thermo Fisher Scientific) and pulsed with either mLAMA4 ($CFSE^{hi}$) or SIINFEKL ($CFSE^{lo}$) peptide, respectively, at 1μM overnight. Cells were washed extensively, combined at a 50:50 ratio in PBS, and $20x10^6$ total cells were injected retro-orbitally into tumor-bearing mice 11 days post tumor transplant. Naïve, non-tumor bearing mice were used as a control. Spleens from tumor-bearing or control naïve animals were harvested 24 hours post cell transfer, stained with Zombie NIR viability dye (Biolegend) and quantified for the presence of CFSE labeled target cells. On histograms, equivalent heights of $CFSE^{hi}$ and $CFSE^{lo}$ peaks indicate equivalent numbers of each cell population are present, and that no cytotoxicity was observed. Peaks that differ in height, where the $CFSE^{lo}$ population is more abundant than the $CFSE^{hi}$ population, indicate that cytotoxicity was observed specifically against the mLAMA4 peptide-pulsed, $CFSE^{hi}$ population of cells. The equation used for calculating % specific lysis was [1-(naïve control ratio/experimental ratio)] x 100 with ratio = irrelevant percentage / specific epitope percentage.

Statistics

Statistical analysis was performed using GraphPad Prism software version 7. Unless otherwise noted, significance was determined with an unpaired, two-tailed Student's t test.

Extended Data

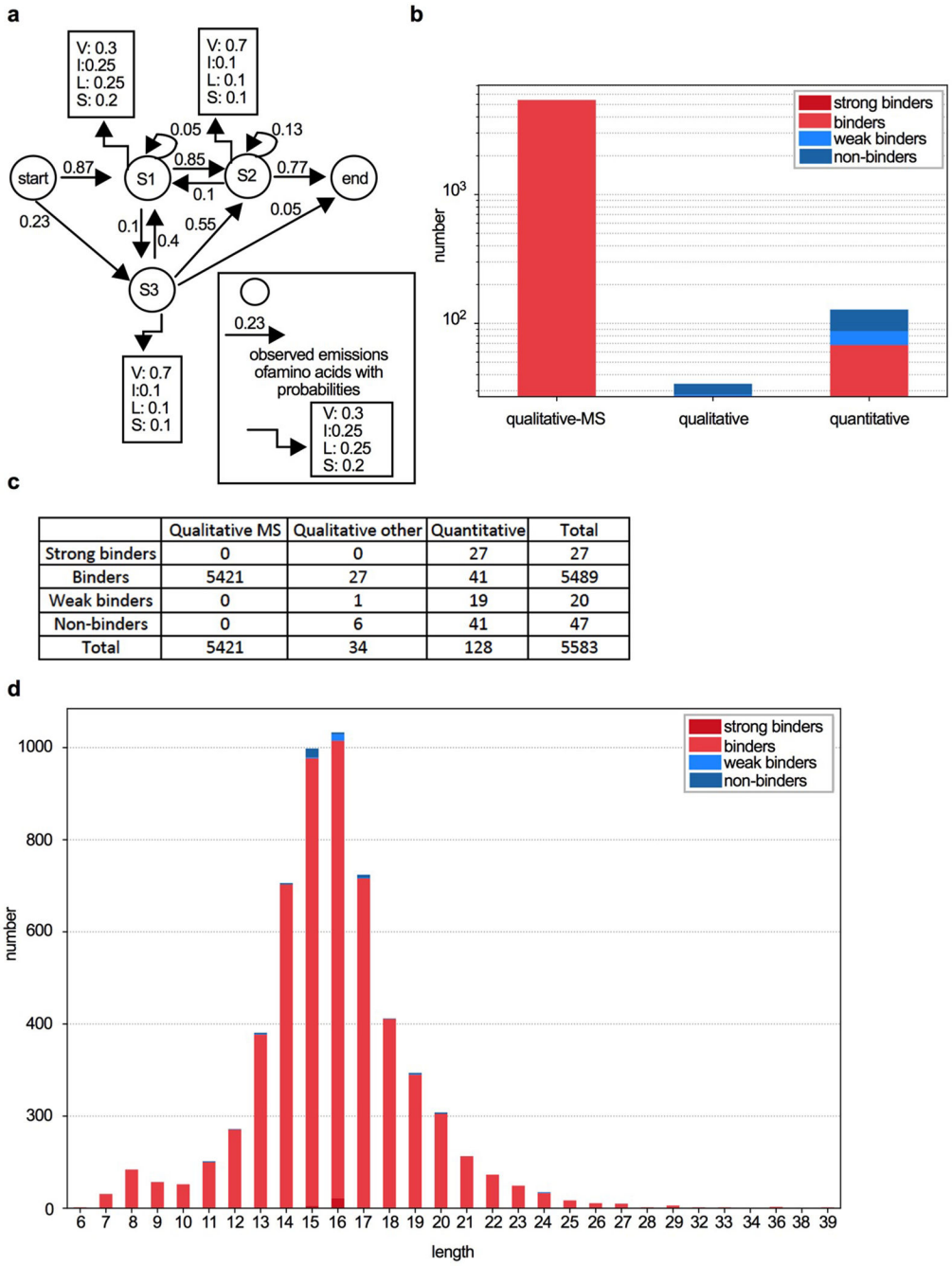

	Qualitative MS	Qualitative other	Quantitative	Total
Strong binders	0	0	27	27
Binders	5421	27	41	5489
Weak binders	0	1	19	20
Non-binders	0	6	41	47
Total	5421	34	128	5583

Extended Data Figure 1: The hmMHC predictive algorithm and IEDB'18 H2-I-A^b training data set composition

(a) An example of a fully-connected hidden Markov model with 3 hidden states, and emissions corresponding to amino acids. (b-d) Composition of IEDB dataset (MHC full ligand export downloaded on 2018-11-25) represented as number of peptides per binding category and measurement type (b, c) and binding category and peptide length (d). Strong binders: IC50 ≤ 50 nM; binders: 50 nM < IC50 ≤ 500nM; weak binders: 500 nM < IC50 ≤ 5000 nM; non-binders: all remaining peptides. MS: mass spectrometry.

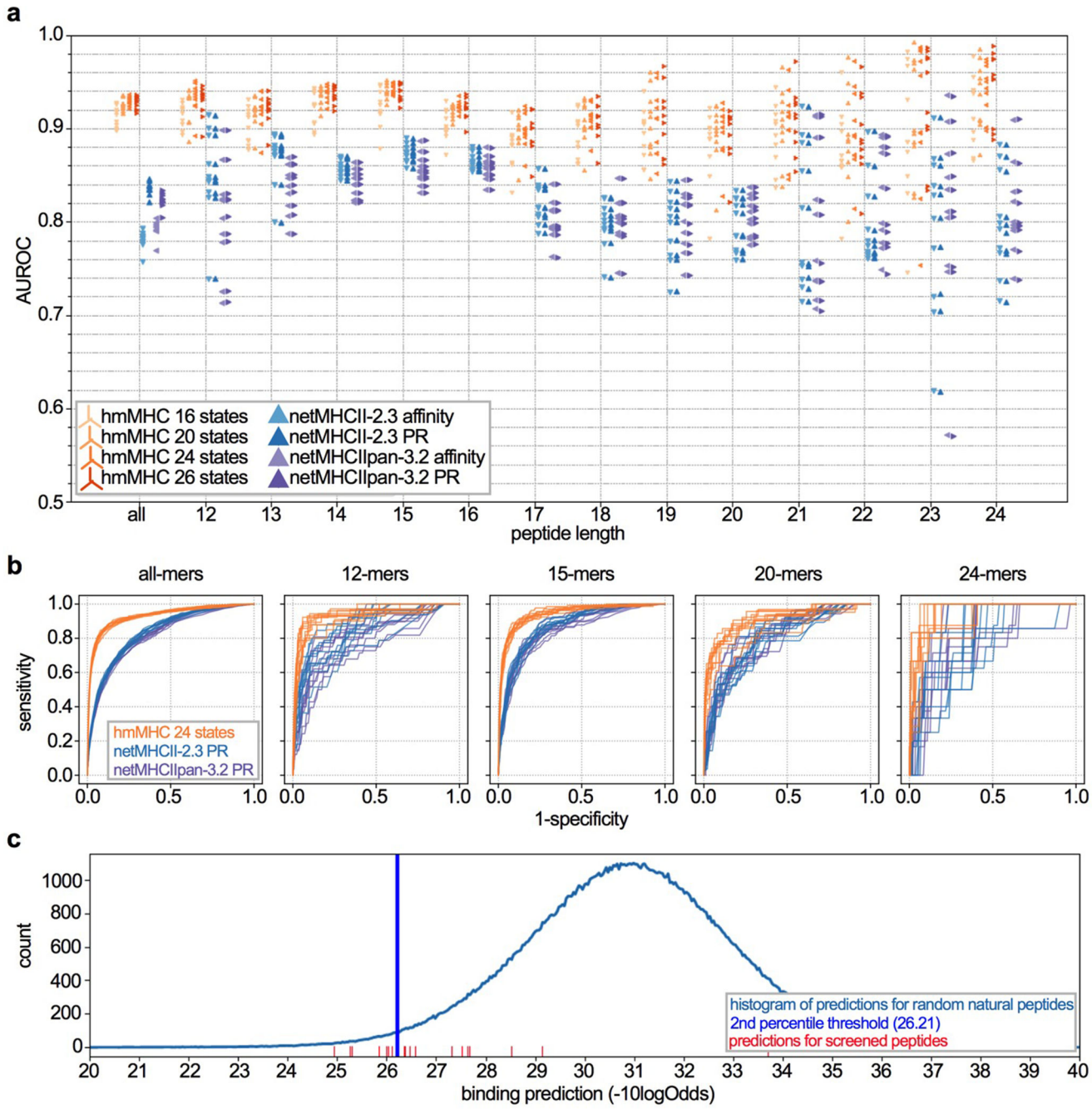

Extended Data Figure 2: Performance of hmMHC compared to netMHCII-2.3 and netMHCIIpan-3.2

(a) hmMHC (orange stars) underwent 10X cross-validation. In each of the 10 cross-validation partitions, on average there were 4,412 binders in the training set, and 771 binders and 77,086 random natural peptides in the validation set. Performance was compared in terms of AUROC to the performance of netMHCII-2.3 (blue triangles) and netMHCIIpan-3.2 (purple triangles) applied on the same validation sets. For hmMHC, performance for different numbers of hidden states is shown. For netMHCII-2.3 and netMHCIIpan-3.2, performance is shown for both predicted affinity and percentile rank

(PR). (b) ROC curves showing performance of hmMHC on H2-I-A^b dataset compared to existing predictors. ROC curves of all peptides and per specific peptide length for every cross-validation partition are shown. (c) Illustration of percentile rank for strong binder classification calibrated on random natural peptides. Red lines indicate the percentile ranks of peptides screened for $CD4^+$ T cell reactivity.

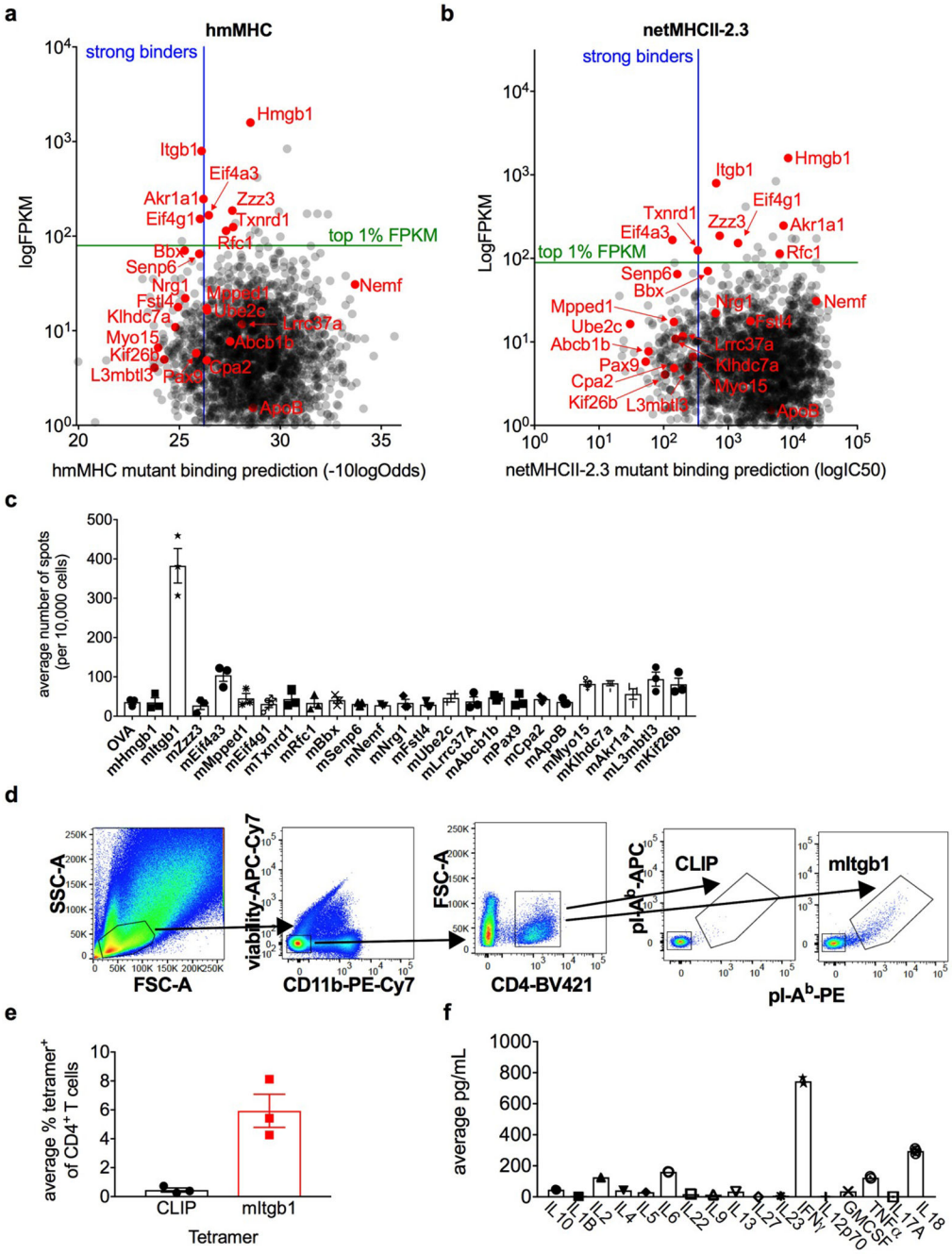

Extended Data Figure 3: mITGB1 is a major MHC class II-restricted neoantigen in T3 sarcomas.

(a-b) T3 MHC-II neoantigen predictions for all expressed mutations were made using hmMHC (a) and netMHCII-2.3 (b) (netMHCIIpan-3.2 predictions yield very similar results). The predictions are shown as −10 log odds predictor value or logIC50 (smaller values indicate higher likelihood of being presented by I-A^b) and expression level (FPKM). Strong binders are defined as mutations residing in the 2nd percentile of I-A^b binding predictions for random natural peptides for each algorithm (−10logOdds ≤ 26.21 or IC50 ≤ 343.8 nM). The N710Y mutation in Itgb1 met the strong binder threshold in the hmMHC

predictions but not in the netMHCII-2.3 predictions. Red dots indicate all mutations that were screened for $CD4^+$ T cell reactivity. Green line denotes high expression cutoff (FPKM=89.1). Blue line indicates strong binder cut off for each algorithm. (c) Two million T3 sarcoma cells were injected subcutaneously into syngeneic mice and $CD4^+$ TIL was isolate on day 12. IFNγ ELISPOT was performed using naïve splenocytes pulsed with 2 μg mL^{-1} of the indicated peptides. Data is shown as average of three independent experiments ± SEM. (d) Gating strategy for pI-A^b tetramer staining of whole TIL. (e) Quantification of mITGB1-tetramer and CLIP-tetramer staining of $CD4^+$ T cells from whole T3 TIL 12 days post-transplant. Data is shown as average percent tetramer-positive cells of $CD4^+$ cells ± SEM of 3 independent experiments. (f) Syngeneic 129S6 mice were injected subcutaneously with $2x10^6$ T3 sarcoma cells and TIL-derived $CD4^+$ T cells were harvested 12 days post transplant. $CD4^+$ T cells were stimulated with naïve splenocytes pulsed with 2 μg/mL $OVA_{323-339}$ control or $mITGB1_{697-724}$ peptide for a flow-based multi-cytokine array. Representative data from one of two independent experiments using pools of 5 tumors each is shown as average of technical triplicate wells from 3 pooled tumors.

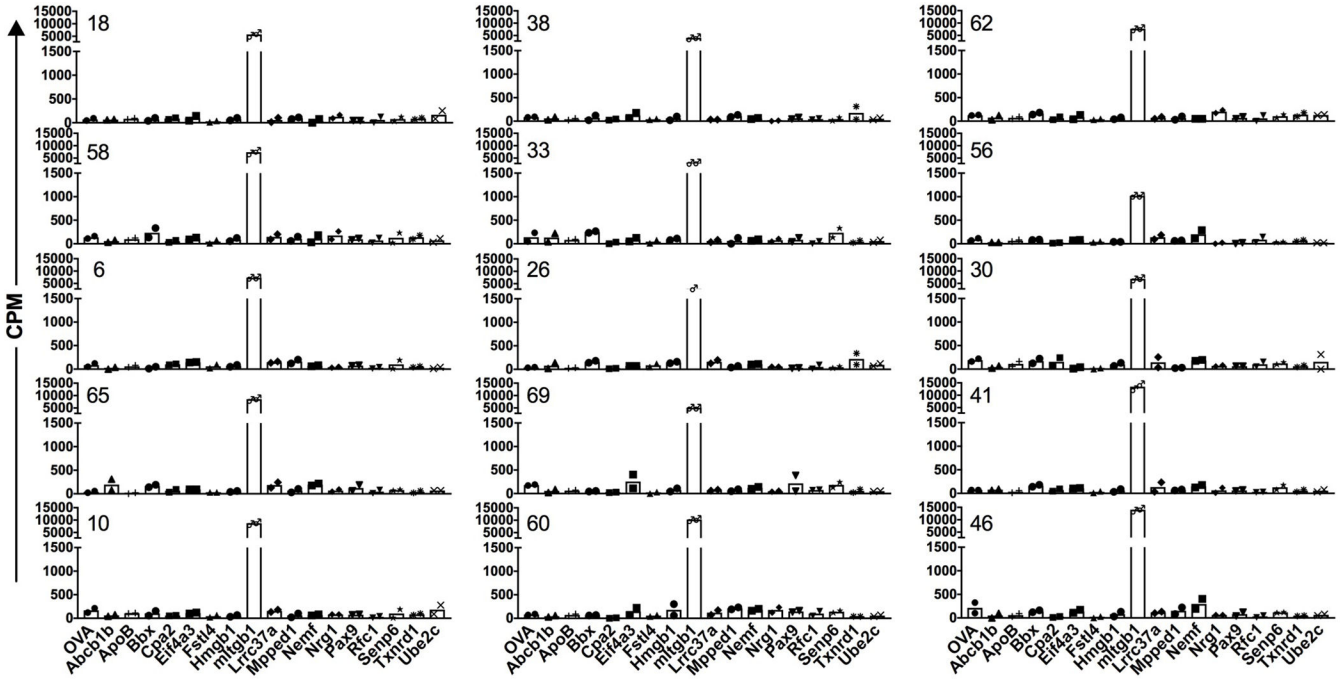

Extended Data Figure 4: T3 TIL-derived CD4$^+$ T cell hybridomas are reactive against mITGB1.

CTLL assay of T3 TIL-derived CD4$^+$ T cell hybridoma lines stimulated with naïve splenocytes pulsed with 2 μg/ml of the individual indicated peptides. Representative data from one of 3 independent experiments is shown as average cpm from technical duplicate wells.

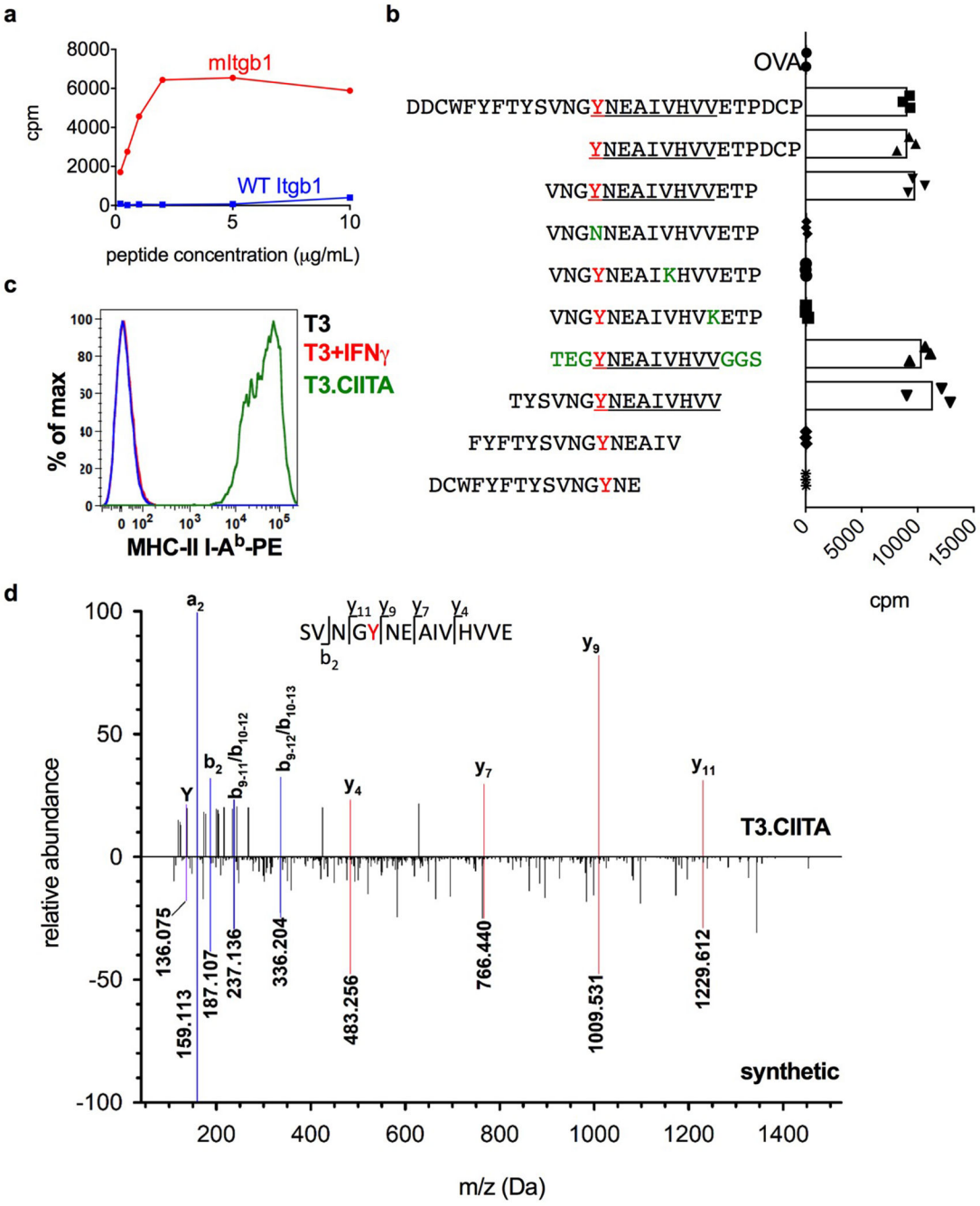

Extended Data Figure 5: The mITGB1 epitope is presented on I-A^{b}.

(d) T3 CD4^{+} T cell hybridomas were stimulated with 2 μg ml^{-1} mITGB1^{710Y} versus WT Itgb1^{710N} peptide-pulsed splenocytes. Activation was measured by CTLL assay. Representative data from three independent hybridoma lines is shown as average of technical replicate wells. (b) Mapping of the mITGB1 MHC class II binding core was performed using the CD4^{+} T cell hybridoma line 41 stimulated with naïve splenocytes pulsed with 2 μg/ml of overlapping peptides covering mITGB1$_{697\text{-}724}$. Red denotes the T3-specific mutant amino acid at position p1 of the minimal epitope; underlined portion denotes

the validated binding core. Green amino acids represent random residue substitutions used to specifically define valines at residues 715 and 718 as the p6 and p9 MHC-II binding positions and the complete MHC-II binding core. Representative data from 2 independent experiments is shown as the average of technical triplicate wells. (c) MHC-II I-A^b staining of parental T3 cells, IFNγ-stimulated T3 cells and T3 cells transduced with a vector encoding CIITA (T3.CIITA). Representative data from one of three independent experiments is shown. (d) Mirror plot showing match between MS/MS spectra of the 14mer peptide sequence encompassing the N710Y of mITGB1 eluted from T3.CIITA cells (positive axis) and a corresponding synthetic peptide (negative axis). Labeled *m/z* values reflect those experimentally observed for the endogenous peptide, with peaks representing *b* ions highlighted in blue and *y* ions in red.

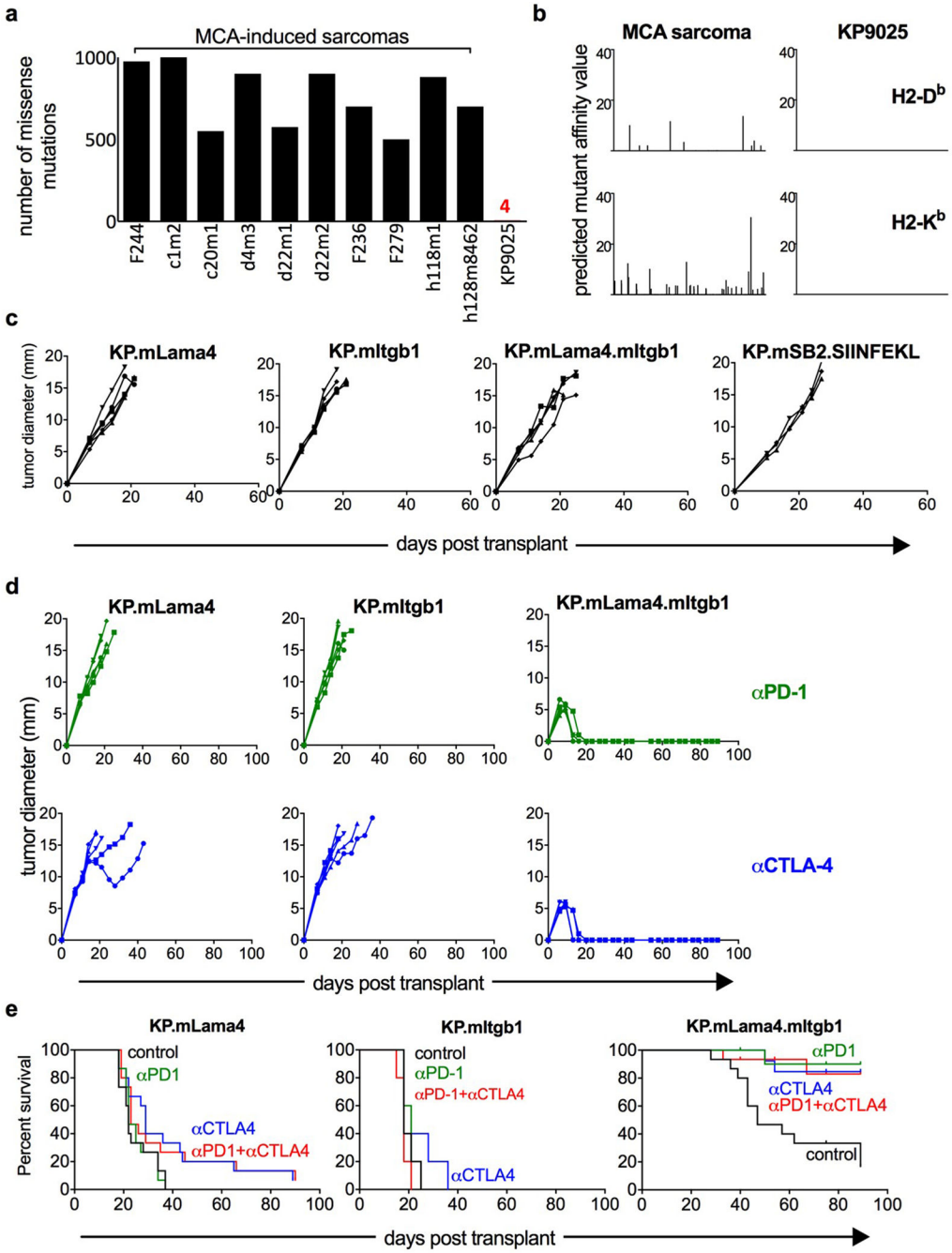

Extended Data Figure 6: mITGB1 CD4$^+$ T cells are required for tumor rejection in response to ICT.

(a) Comparison of total number of expressed missense mutations between 10 different MCA-induced sarcomas and KP9025. Mutations were defined by WES and RNAseq and mutational load is shown on a per cell basis. (b) Comparison of predicted neoantigen MHC-I affinity values between KP9025 and MCA-induced sarcoma F244 for H-2D^b (top) and H-2K^b (bottom). KP9025 were not predicted to express any MHC-I neoantigens. (c) Rag2$^{-/-}$ mice were subcutaneously injected with 1x10^6 KP.mLAMA4, KP.mITGB1, KP.mLAMA4.mITGB1 or KP.mSB2.SIINFEKL. Representative data from one of two

independent experiments is presented as tumor diameter of individual mice (n=5 KP.mLAMA4, KP.mITGB1 and KP.mLAMA4.mITGB1 and n=3 KP.mSB2.SIINFEKL mice per group per experiment) (d) WT syngeneic 129S4 mice were injected subcutaneously with $1x10^6$ KP.mLAMA4, KP.mITGB1 or KP.mLAMA4.mITGB1 and treated with αPD-1 (top) or αCTLA single agent ICT (bottom) on days 3, 6, and 9 post transplant. Representative data from one of three independent experiments is shown as tumor diameter from individual mice (n=5 in all groups per experiment). (e) Survival curves from all experiments described in (d) and Figure 2e (n=15 in all groups).

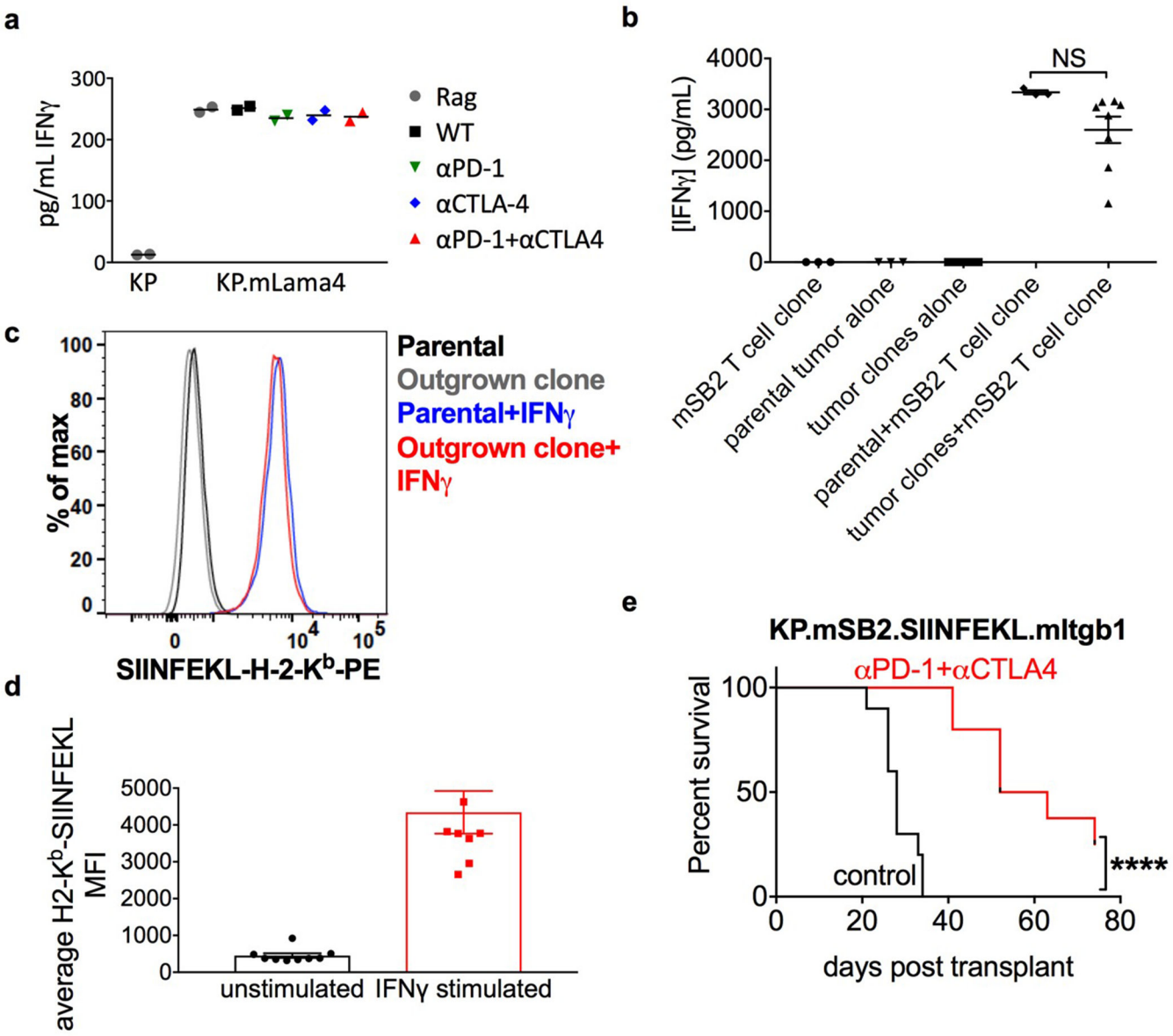

Extended Data Figure 7: Outgrowth of nonimmunogenic sarcoma cells expressing MHC-I neoantigens is not a result of cancer immunoediting.

(a) Rag2$^{-/-}$ or WT 129S4 mice were injected with 1x10^6 KP9025 or KP.mLAMA4 cells and treated with αPD-1, αCTLA or αPD-1 + αCTLA4 on days 3, 6 and 9. Tumors were harvested once the average diameter reached 20 mm and sarcoma cell lines were established *ex vivo*. Cell lines were stimulated with IFNγ to upregulate MHC-I and subsequently used to stimulate the mLAMA4-specific CD8$^+$ 74.14 T cell clone. IFNγ secretion by T cells was measured by ELISA. Representative data from 2 independent experiments is represented as the average of 2 independent tumor samples in each group. (b) WT 129S4 mice were injected with 1x10^6 KP.mSB2.SIINFEKL cells and treated with αPD-1+αCTLA4 combination ICT on days 3, 6 and 9. Tumors were harvested as described in (a). Established *ex vivo* cell lines were cloned via limiting dilution and parental KP.mSB2.SIINFEKL cells or individual clones from outgrown tumors were used to stimulate the mSB2-specific C3

$CD8^+$ T cell clone and IFNγ production quantified by ELISA. Representative data from four independent experiments is presented as average IFNγ concentration of 8 individual clones ± SEM. Significance was determine using an unpaired, two sided t test. (c) Cell surface staining of SIINFEKL-H-2-K^b expressed by unstimulated or IFNγ-stimulated parental KP.mSB2.SIINFEKL or individual clones described in (b). A representative histogram is shown. (d) Quantification of average SIINFEKL-H-2-K^b MFI from 8 individual clones described in (c) ± SEM. NS not significant. (e) Survival curves of WT 129S4 mice injected subcutaneously with $1x10^6$ KP.mSB2.SIINFEKL.mITGB1. Mice were treated with control mAb or αPD-1+αCTLA4 combination ICT on days 3, 6 and 9. n=10 mice per group from two independent experiments. ****indicates $p=1.5x10^{-5}$ as calculated using Mantel-Cox test.

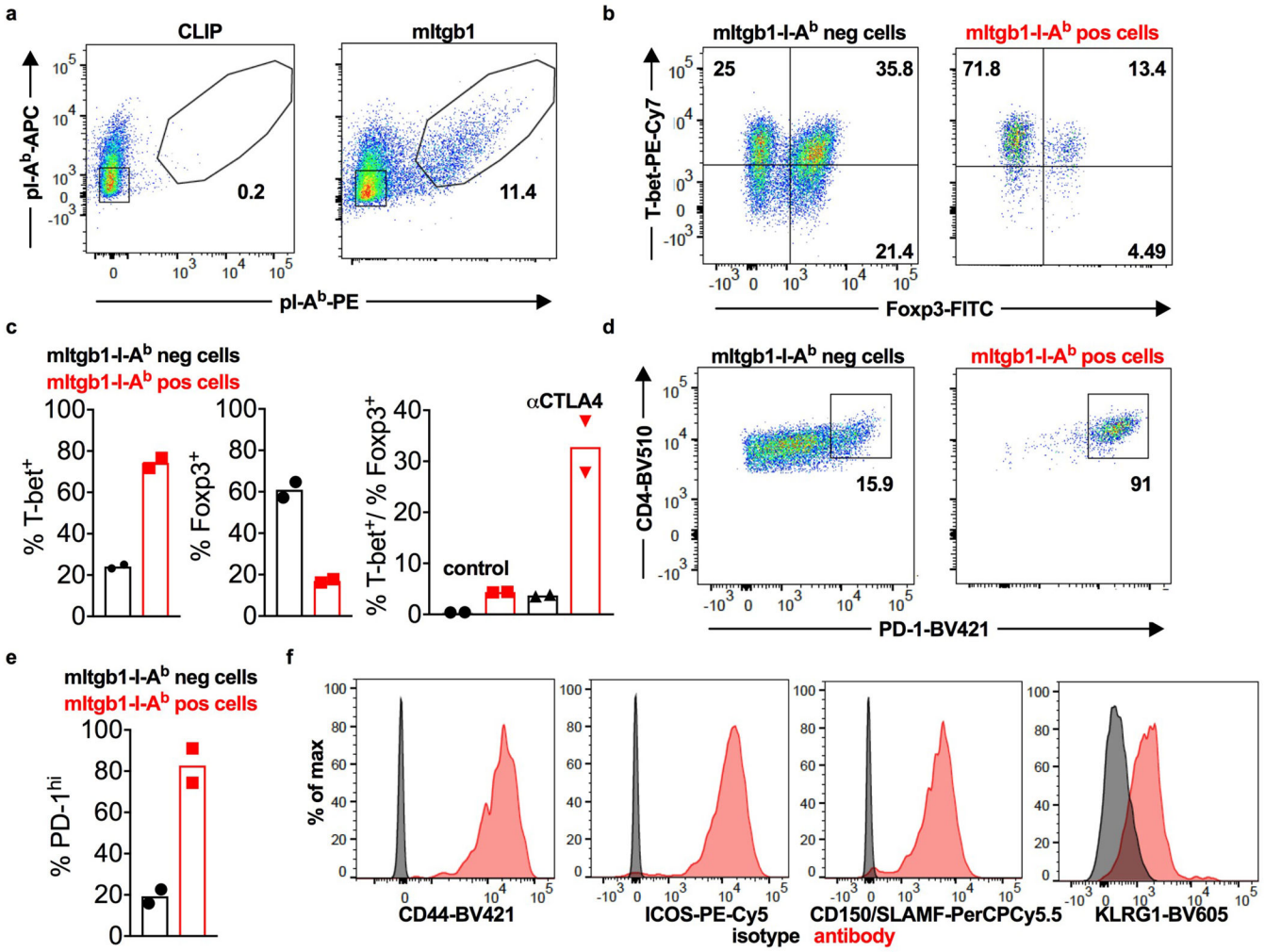

Extended Data Figure 8: mITGB1-specific CD4$^+$ T cells display an activated Th1 phenotype.

(a) Whole TIL from KP.mLAMA4.mITGB1 tumors 12 days post transplant were stained with mITGB1-I-A^b tetramers. Populations were previously gated on viable CD11b$^-$CD4$^+$ cells. Representative data from one of two independent experiments of 5 pooled tumors each is shown. (b) mITGB1-I-A^b tetramer-negative and tetramer-positive cells described in (a) were analyzed for expression of T-BET and FOXP3. Representative plots are shown. (c) Quantification of two independent experiments described in (b) is shown as average percent of tetramer-negative and tetramer-positive cells staining positive for the indicated protein. Tumor-bearing animals received control mAb or α-CTLA4 treatment on days 3, 6, and 9-post transplant where indicated. (d) mITGB1-I-A^b tetramer-positive and tetramer-negative cells described in (a) were analyzed for expression of PD-1. Representative plots are shown. (e) Quantification of two independent experiments described in (d) is shown as average percent of tetramer-negative and tetramer-positive cells staining positive for PD-1. (f) mITGB1-I-A^b tetramer-positive cells described in (a) were analyzed for expression of the indicated proteins. Representative histograms from one of two independent experiments using pools of 5 tumors each are shown.

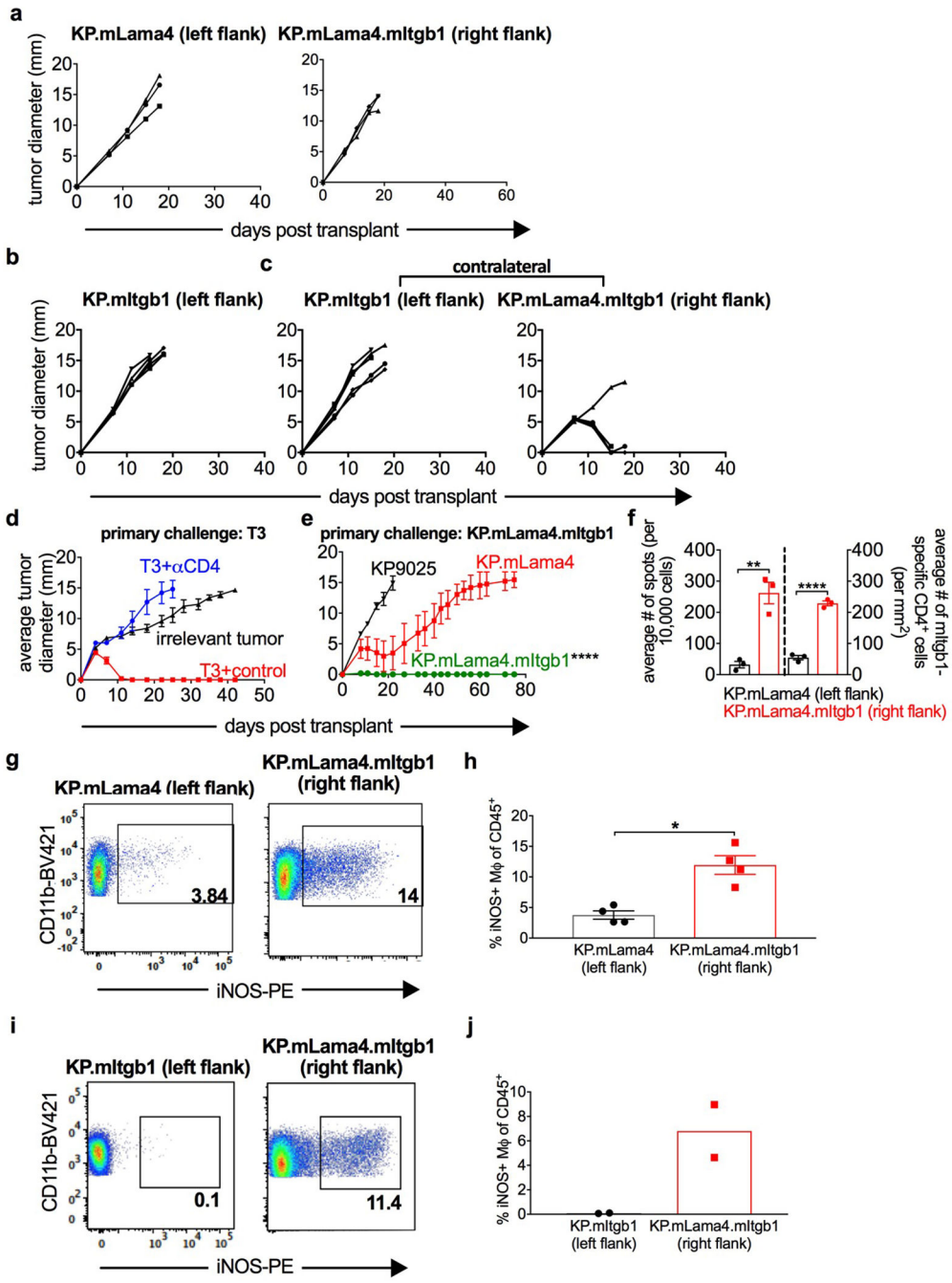

Extended Data Figure 9: CD4$^+$ T cell help is required at the tumor site during primary and memory responses.

(a) Rag2$^{-/-}$ mice were simultaneously injected with 1x10^6 KP.mLAMA4 and KP.mLAMA4.mITGB1 cells on contralateral flanks. Representative data from one of two independent experiments is shown as individual tumor diameter (n=3 in each experiment). (b) WT 129S4 mice were injected with 1x10^6 KP.mITGB1 cells and were treated with αPD-1+αCTLA4 combination ICT on days 3, 6, and 9. Representative data from one of two individual experiments is shown as individual tumor diameters (n=5 in all experiments). (c) WT 129S4 mice were simultaneously injected with 1x10^6 KP.mLAMA4 and

KP.mLAMA4.mITGB1 cells on contralateral flanks and treated as in (b). Representative data from one of two individual experiments is shown as individual tumor diameters (n=5 in all experiments). (d) WT 129S6 mice were injected subcutaneously with $2x10^6$ T3 sarcoma cells and were treated with αPD-1+αCTLA4 combination ICT on days 3, 6, and 9. Following tumor rejection and a 30-day recovery period, tumor-experienced mice were rechallenged with $2x10^6$ T3 cells in the presence of control mAb or CD4-depleting antibody, or with irrelevant sarcoma cells. Representative data from one of two independent experiments are shown as average tumor diameter ± SEM (n=5 in all groups per experiment). (e) WT 129S4 mice were injected subcutaneously with $1x10^6$ KP.mLAMA4.mITGB1 cells followed by surgical resection 10 days post transplant. After a 30-day recovery period, tumor-experienced mice were rechallenged with $1x10^6$ KP9025, KP.mLAMA4.mITGB1, or KP.mLAMA4. Representative data from one of two independent experiments are shown as average tumor diameter ± SEM (n=5 in all groups per experiment). ****indicates $p=2x10^{-6}$ as calculated using a 2-way ANOVA with multiple comparisons corrected with the Bonferroni method. (f) Quantification of data from three independent experiments described in Figure 5c is shown as average number of spots ± SEM (left) and average number of mITGB1-specific $CD4^+$ cells ± SEM (right). **indicates p=.003, ****indicates $p=7.2x10^{-5}$ (unpaired, two sided t test). (g) $CD45^+Ly6G^-MHCII^+CD64^+CD25^-CD11b^+F4/80^+$ macrophages in TIL from animals bearing the indicated contralateral tumors were analyzed for expression of iNOS 11 days post tumor transplant. Representative data is shown. (h) Quantification of $iNOS^+$ macrophages from experiments described in (f) as a percent of total $CD45^+$ cells. Data is shown as average ± SEM of four independent experiments. *indicates p=.03 as calculated using an unpaired, two sided t test. (i) $CD45^+Ly6G^-MHCII^+CD64^+CD25^-CD11b^+F4/80^+$ macrophages from the indicated contralateral tumors described were isolated 11-days post transplant and analyzed for expression of iNOS. Representative plots are shown. (j) Quantification of $iNOS^+$ macrophages from two independent experiments described in (h) is shown as average percent of total $CD45^+$ cells.

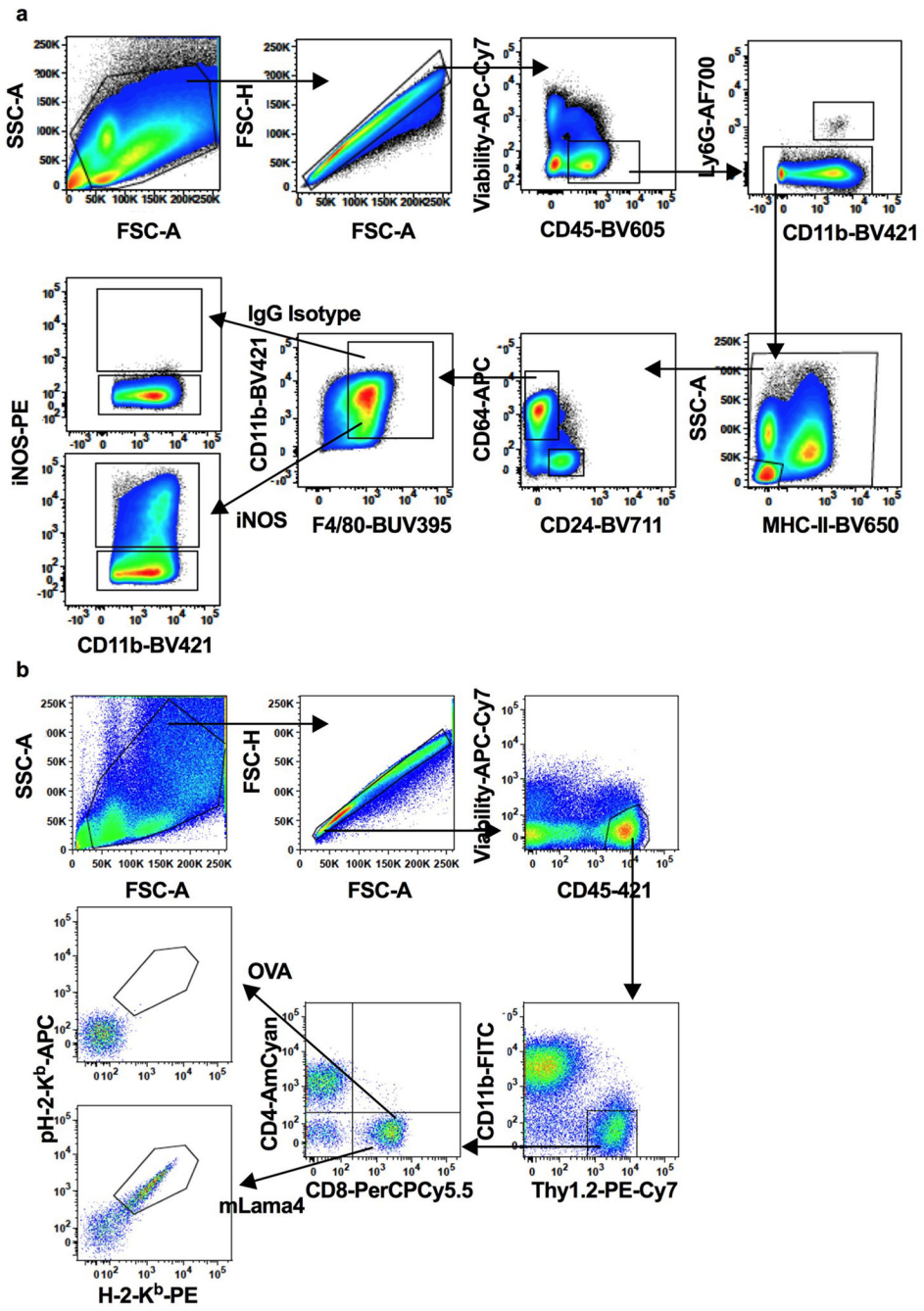

Extended Data Figure 10: Gating strategies for multi-color flow cytometry.

Gating strategies for multi-color flow cytometry analysis of tumor-infiltrating (a) macrophage and (b) T cell populations.

Supplementary Material

Refer to Web version on PubMed Central for supplementary material.

ACKNOWLEDGEMENTS

The authors thank all members of the Schreiber lab for helpful discussions and technical support. This work was supported by grants to R.D.S. from the National Cancer Institute of the National Institutes of Health (RO1CA190700), the Parker Institute for Cancer Immunotherapy, the Cancer Research Institute, Janssen Pharmaceutical Company of Johnson and Johnson, the Prostate Cancer Foundation, and by a Stand Up to Cancer-Lustgarten Foundation Pancreatic Cancer Foundation Convergence Dream Team Translational Research Grant. Stand Up to Cancer is a program of the Entertainment Industry Foundation administered by the American Association for Cancer Research. E.A. and D.M.L were supported by a postdoctoral training grant (T32 CA00954729) from the National Cancer Institute. D.M.L. and M.M.G. were supported by the Irvington Postdoctoral Fellowship from the Cancer Research Institute. M.D. is a St. Baldrick's Scholar with support from Hope with Hazel and a Pew-Stewart Scholar for Cancer Research supported by the Pew Charitable Trusts. J.P.W. is supported by the National Cancer Institute of the National Institutes of Health Paul Calabresi Career Development Award in Clinical Oncology (K12CA167540). M.M.G. is supported by a Parker Bridge Scholar Award from the Parker Institute for Cancer Immunotherapy. K.W.W. receives support from the National Institutes of Health (R01CA238039). T.J. receives support from a National Institutes of Health Cancer Center Support Grant (P30CA14051) and the Howard Hughes Medical Institute. E.R.U. receives support from the National Institute of Diabetes and Digestive and Kidney Diseases of the National Institutes of Health (AI114551 and DK058177). Aspects of the studies including ELISPOT were performed by Diane Bender at the Immunomonitoring Laboratory (IML), which is supported by the Andrew M. and Jane N. Bursky Center for Human Immunology and Immunotherapy Programs and the Alvin J. Siteman Comprehensive Cancer Center which, in turn, is supported by the National Cancer Institute of the National Institutes of Health Cancer Center Support Grant (P30CA91842).

REFERENCES

1. Schreiber RD, Old LJ & Smyth MJ Cancer immunoediting: integrating immunity's roles in cancer suppression and promotion. Science 331, 1565–1570 (2011). [PubMed: 21436444]
2. Larkin J et al. Combined Nivolumab and Ipilimumab or Monotherapy in Untreated Melanoma. N. Engl. J. Med 373, 23–34 (2015). [PubMed: 26027431]
3. Motzer RJ et al. Nivolumab versus Everolimus in Advanced Renal-Cell Carcinoma. N. Engl. J. Med 373, 1803–1813 (2015). [PubMed: 26406148]
4. Borghaei H et al. Nivolumab versus Docetaxel in Advanced Nonsquamous Non-Small-Cell Lung Cancer. N. Engl. J. Med 373, 1627–1639 (2015). [PubMed: 26412456]
5. Lennerz V et al. The response of autologous T cells to a human melanoma is dominated by mutated neoantigens. Proc. Natl. Acad. Sci. U. S. A 102, 16013–16018 (2005). [PubMed: 16247014]
6. Matsushita H et al. Cancer exome analysis reveals a T-cell-dependent mechanism of cancer immunoediting. Nature 482, 400–404 (2012). [PubMed: 22318521]
7. DuPage M, Mazumdar C, Schmidt LM, Cheung AF & Jacks T Expression of tumour-specific antigens underlies cancer immunoediting. Nature 482, 405–409 (2012). [PubMed: 22318517]
8. Robbins PF et al. Mining exomic sequencing data to identify mutated antigens recognized by adoptively transferred tumor-reactive T cells. Nat. Med 19, 747–752 (2013). [PubMed: 23644516]
9. Gubin MM et al. Checkpoint blockade cancer immunotherapy targets tumour-specific mutant antigens. Nature 515, 577–581 (2014). [PubMed: 25428507]
10. Wölfel T et al. A p16INK4a-insensitive CDK4 mutant targeted by cytolytic T lymphocytes in a human melanoma. Science 269, 1281–1284 (1995). [PubMed: 7652577]
11. Snyder A et al. Genetic Basis for Clinical Response to CTLA-4 Blockade in Melanoma. N. Engl. J. Med 371, 2189–2199 (2014). [PubMed: 25409260]
12. Strønen E et al. Targeting of cancer neoantigens with donor-derived T cell receptor repertoires. Science 352, 1337–1341 (2016). [PubMed: 27198675]
13. Rizvi NA et al. Cancer immunology. Mutational landscape determines sensitivity to PD-1 blockade in non-small cell lung cancer. Science 348, 124–128 (2015). [PubMed: 25765070]
14. Van Allen EM et al. Genomic correlates of response to CTLA-4 blockade in metastatic melanoma. Science 350, 207–211 (2015). [PubMed: 26359337]
15. Spranger S et al. Density of immunogenic antigens does not explain the presence or absence of the T-cell-inflamed tumor microenvironment in melanoma. Proc. Natl. Acad. Sci. U. S. A 113, E7759–E7768 (2016). [PubMed: 27837020]

16. Hugo W et al. Genomic and Transcriptomic Features of Response to Anti-PD-1 Therapy in Metastatic Melanoma. Cell 165, 35–44 (2016). [PubMed: 26997480]
17. Hellmann MD et al. Genomic Features of Response to Combination Immunotherapy in Patients with Advanced Non-Small-Cell Lung Cancer. Cancer Cell 33, 843–852.e4 (2018). [PubMed: 29657128]
18. Kreiter S et al. Mutant MHC class II epitopes drive therapeutic immune responses to cancer. Nature 520, 692–696 (2015). [PubMed: 25901682]
19. Ott PA et al. An immunogenic personal neoantigen vaccine for patients with melanoma. Nature 547, 217–221 (2017). [PubMed: 28678778]
20. Ossendorp F, Mengedé E, Camps M, Filius R & Melief CJ Specific T helper cell requirement for optimal induction of cytotoxic T lymphocytes against major histocompatibility complex class II negative tumors. J. Exp. Med 187, 693–702 (1998). [PubMed: 9480979]
21. Corthay A et al. Primary antitumor immune response mediated by CD4+ T cells. Immunity 22, 371–383 (2005). [PubMed: 15780993]
22. Wong SBJ, Bos R & Sherman LA Tumor-specific CD4+ T cells render the tumor environment permissive for infiltration by low-avidity CD8+ T cells. J. Immunol. Baltim. Md 1950 180, 3122–3131 (2008).
23. Bos R & Sherman LA CD4+ T-cell help in the tumor milieu is required for recruitment and cytolytic function of CD8+ T lymphocytes. Cancer Res. 70, 8368–8377 (2010). [PubMed: 20940398]
24. Zhu Z et al. CD4+ T Cell Help Selectively Enhances High-Avidity Tumor Antigen-Specific CD8+ T Cells. J. Immunol. Baltim. Md 1950 195, 3482–3489 (2015).
25. Borst J, Ahrends T, Bąbała N, Melief CJM & Kastenmüller W CD4+ T cell help in cancer immunology and immunotherapy. Nat. Rev. Immunol 18, 635–647 (2018). [PubMed: 30057419]
26. Andreatta M et al. An automated benchmarking platform for MHC class II binding prediction methods. Bioinforma. Oxf. Engl 34, 1522–1528 (2018).
27. Mittal P et al. Tumor-Unrelated CD4 T Cell Help Augments CD134 plus CD137 Dual Costimulation Tumor Therapy. J. Immunol. Baltim. Md 1950 195, 5816–5826 (2015).
28. Suri A, Walters JJ, Rohrs HW, Gross ML & Unanue ER First Signature of Islet β-Cell-Derived Naturally Processed Peptides Selected by Diabetogenic Class II MHC Molecules. J. Immunol 180, 3849–3856 (2008). [PubMed: 18322192]
29. Tran E et al. Cancer immunotherapy based on mutation-specific CD4+ T cells in a patient with epithelial cancer. Science 344, 641–645 (2014). [PubMed: 24812403]
30. Linnemann C et al. High-throughput epitope discovery reveals frequent recognition of neo-antigens by CD4+ T cells in human melanoma. Nat. Med 21, 81–85 (2015). [PubMed: 25531942]
31. Old LJ & Boyse EA Immunology of Experimental Tumors. Annu. Rev. Med 15, 167–186 (1964). [PubMed: 14139934]
32. Wei SC et al. Distinct Cellular Mechanisms Underlie Anti-CTLA-4 and Anti-PD-1 Checkpoint Blockade. Cell 170, 1120–1133.e17 (2017). [PubMed: 28803728]
33. Gubin MM et al. High-Dimensional Analysis Delineates Myeloid and Lymphoid Compartment Remodeling during Successful Immune-Checkpoint Cancer Therapy. Cell 175, 1443 (2018). [PubMed: 30445041]
34. Marzo AL et al. Tumor-Specific CD4+ T Cells Have a Major “Post-Licensing” Role in CTL Mediated Anti-Tumor Immunity. J. Immunol 165, 6047–6055 (2000). [PubMed: 11086036]
35. Bennett SRM, Carbone FR, Karamalis F, Miller JFAP & Heath WR Induction of a CD8+ Cytotoxic T Lymphocyte Response by Cross-priming Requires Cognate CD4+ T Cell Help. J. Exp. Med 186, 65–70 (1997). [PubMed: 9206998]
36. Corthay A, Lundin KU, Lorvik KB, Hofgaard PO & Bogen B Secretion of tumor-specific antigen by myeloma cells is required for cancer immunosurveillance by CD4+ T cells. Cancer Res. 69, 5901–5907 (2009). [PubMed: 19567679]

METHODS ONLY REFERENCES

37. Mamitsuka H Predicting peptides that bind to MHC molecules using supervised learning of hidden Markov models. Proteins 33, 460–474 (1998). [PubMed: 9849933]
38. Welch LR Hidden Markov Models and the Baum-Welch Algorithm. IEEE Inf. Theory Soc. Newsl 53, 10–13 (2003).
39. Jurtz V et al. NetMHCpan-4.0: Improved Peptide-MHC Class I Interaction Predictions Integrating Eluted Ligand and Peptide Binding Affinity Data. J. Immunol. Baltim. Md 1950 199, 3360–3368 (2017).
40. Jensen KK et al. Improved methods for predicting peptide binding affinity to MHC class II molecules. Immunology 154, 394–406 (2018). [PubMed: 29315598]
41. Kowalewski DJ & Stevanović S Biochemical large-scale identification of MHC class I ligands. Methods Mol. Biol. Clifton NJ 960, 145–157 (2013).
42. Tungatt K et al. Antibody stabilization of peptide-MHC multimers reveals functional T cells bearing extremely low-affinity TCRs. J. Immunol. Baltim. Md 1950 194, 463–474 (2015).

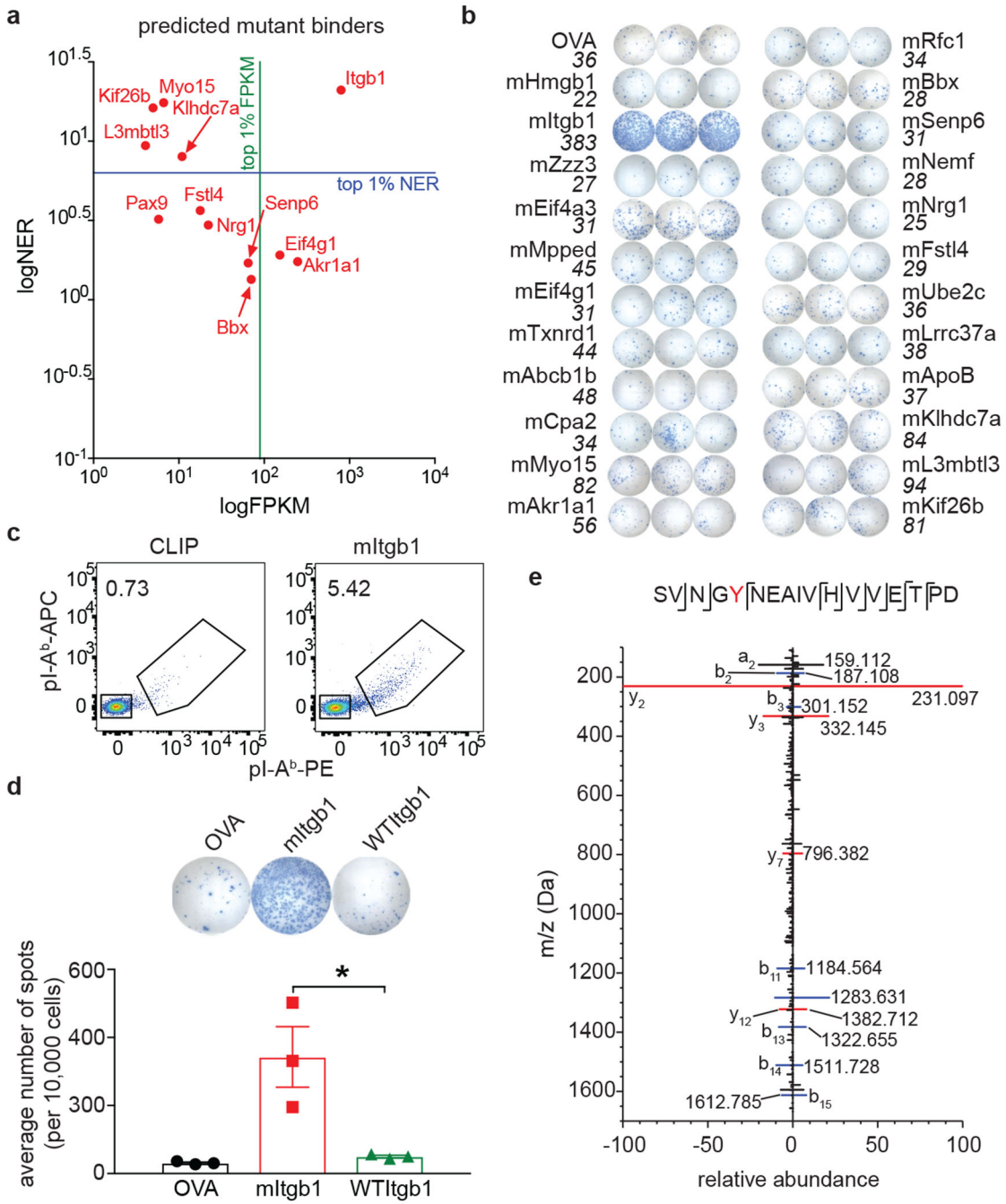

Figure 1: N710Y Itgb1 (mITGB1) is a major MHC class II-restricted neoantigen of T3 sarcoma cells.

(a) hmMHC predictions of MHC-II neoantigens expressed in T3 sarcoma cells. Potential neoantigens were filtered as in Extended Data Fig. 3a and those meeting the strong binder threshold are shown as expression level (FPKM) and neoepitope ratio (NER). Strong binders are those with −10logOdds ≤ 26.21. Green line: high expression cutoff (FPKM=89.1). Blue line: high NER cutoff (NER=6.55). (b) $CD4^+$ T cells isolated from T3 TIL 12 days post-transplant were stimulated in IFNγ ELISPOT analysis with naïve splenocytes pulsed with 2 μg/mL of the indicated individual peptide. Numbers in italics are average number of spots

from three independent experiments. (c) I-A^b tetramer staining of $CD4^+$ T cells from whole T3 TIL 12 days post-transplant. Cells were gated on viable $CD11b^-CD4^+$ cells. Representative data from one of three independent experiments is shown. (d) Freshly isolated $CD4^+$ T cells from day 12 TIL were stimulated with 2 μg ml^{-1} $mITGB1^{710Y}$ or WT $Itgb1^{710N}$ peptide-pulsed splenocytes and analyzed by IFNγ ELISPOT. Data are average ± SEM (n=3 independent experiments). *indicates p=0.03 (unpaired, two sided t test). (e) Mirror plot showing match between MS/MS spectra of the 17mer peptide encompassing $mITGB1^{N710Y}$ eluted from T3.CIITA cells (right) and a corresponding synthetic peptide (left). Labeled *m/z* values reflect those experimentally observed for the endogenous peptide, with peaks representing *b* ions in blue and *y* ions in red.

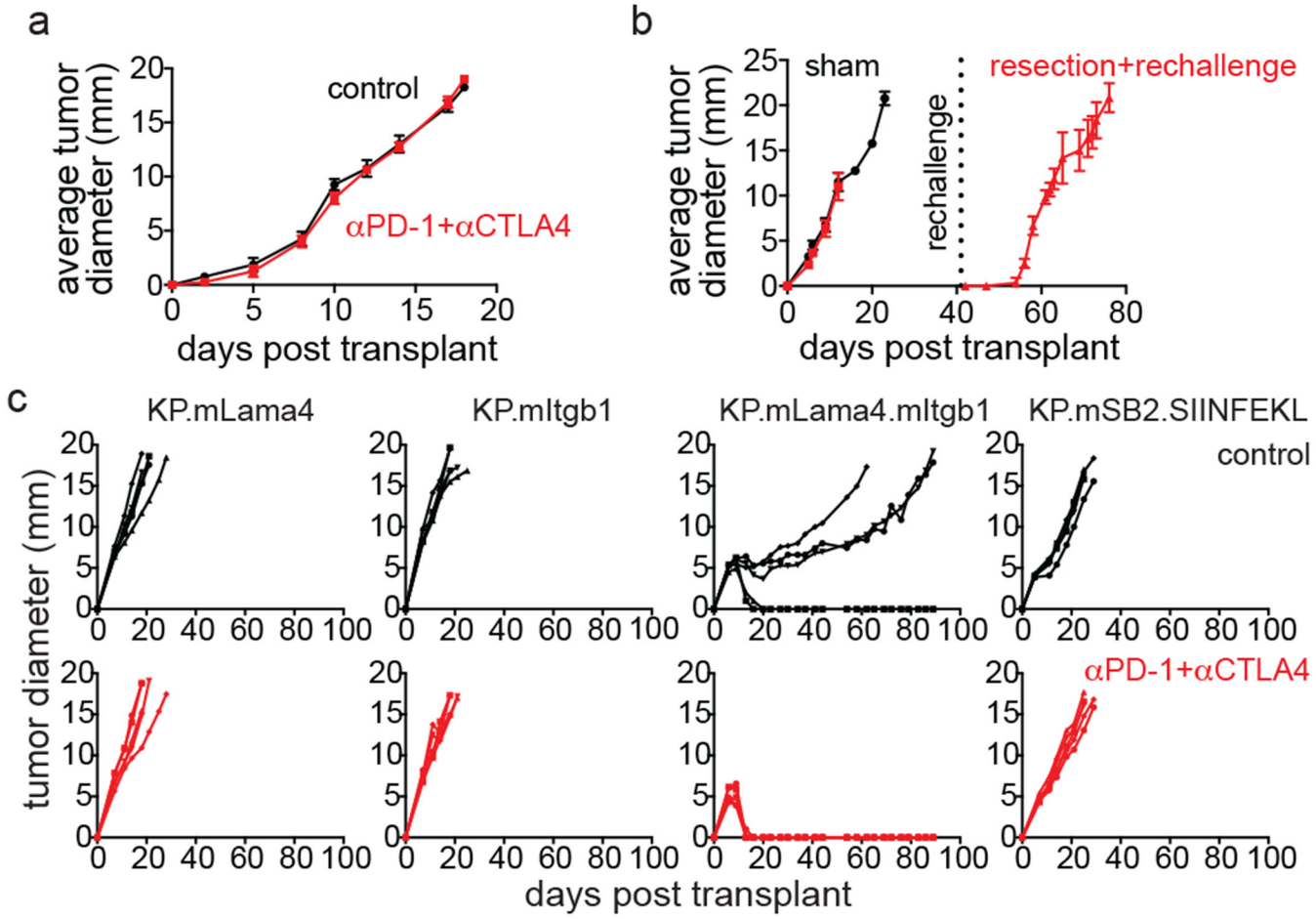

Figure 2: ICT-mediated rejection of a nonimmunogenic sarcoma requires CD4$^+$ and CD8$^+$ T cells.

(a) One million KP9025 sarcoma cells were injected subcutaneously into syngeneic 129S4 mice and animals were treated with either control mAb or the αPD-1+αCTLA4 combination on days 3, 6, and 9 post transplant. Representative data from two independent experiments are shown as average tumor diameter ± SEM (n=5 in all groups per experiment). (b) KP9025 sarcoma cells were injected as above and tumors were surgically resected followed by rechallenge with the same line. Representative data from one of two independent experiments are shown as average tumor diameter ± SEM (n=3 in all groups per experiment). (c) Cohorts of 5 mice were injected with 1x10^6 KP.mLAMA4, KP.mITGB1, KP.mLAMA4.mITGB1, or KP.mSB2.SIINFEKL and treated with either control mAb (top) or the αPD-1 + αCTLA4 combination (bottom) on days 3, 6, and 9 post transplant. Representative data from one of three independent experiments is shown as individual tumor diameters.

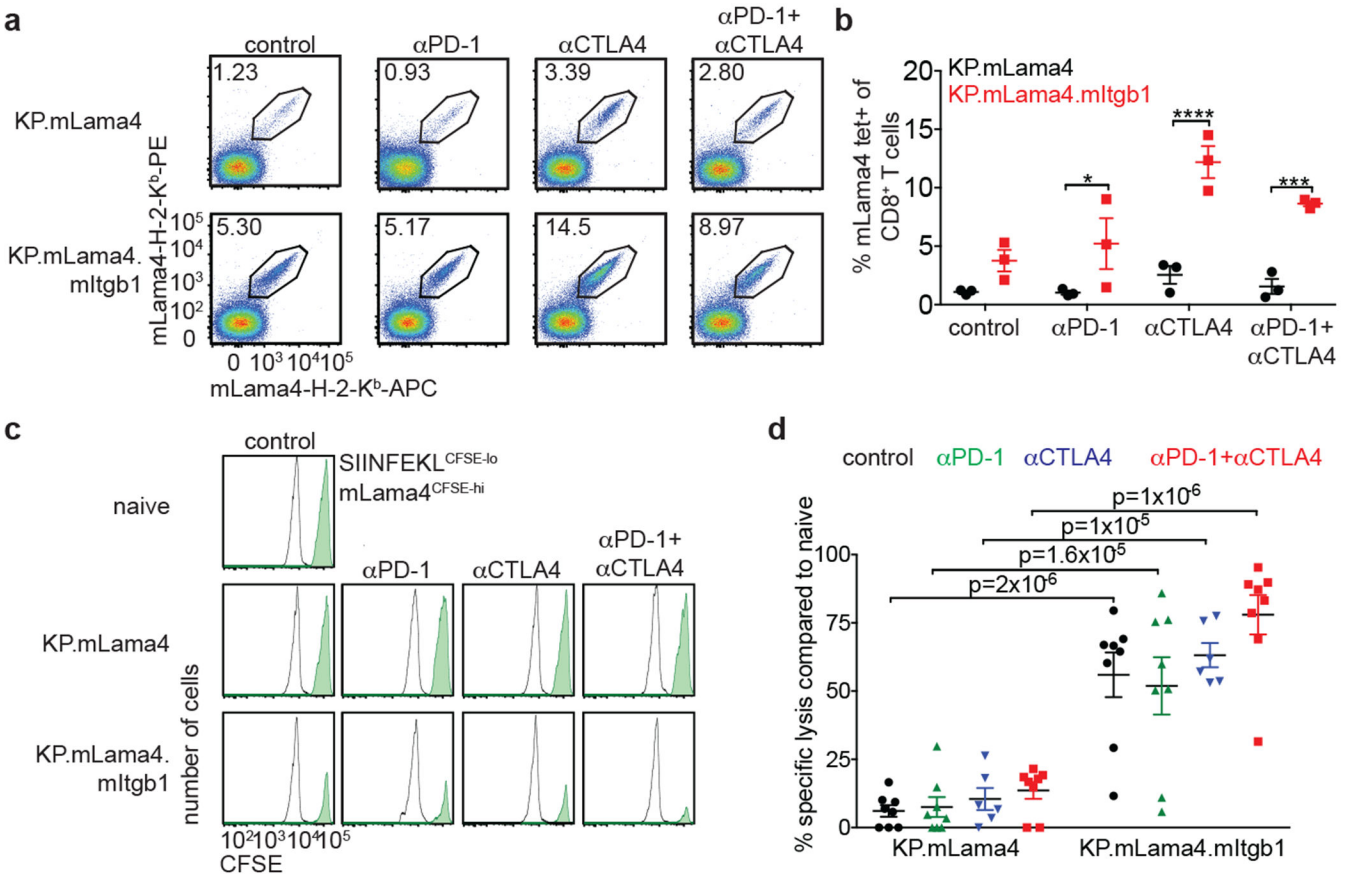

Figure 3: CD4$^+$ T cell help is required for the generation of functional CD8$^+$ CTL during ICT.

(a) Representative tetramer staining of mLAMA4-specific CD8$^+$ T cells from the spleens of KP.mLAMA4 (left) or KP.mLAMA4.mITGB1 (right) tumor-bearing mice 12 days post transplant. Mice received the indicated ICT treatment on days 3, 6, and 9. Cells were gated from viable CD45$^+$CD11b$^-$ Thy1.2$^+$ cells. (b) Quantification of three independent experiments described above is shown as average percent mLAMA4 tetramer-positive of CD8$^+$ T cells ± SEM. *indicates p=.04, ***indicates p=.0007 and ****indicates p=.00003 (2-way ANOVA with multiple comparisons corrected with the Bonferroni method). (c) *In vivo* cytotoxic function of mLAMA4-specific CD8$^+$ T cells. Naïve splenocytes were labeled with 0.5 μM CFSE and pulsed with 1 μM SIINFEKL peptide (white histograms) or 5 μM CFSE and pulsed with 1 μM mLAMA4 peptide (green histograms) and transferred into control naïve or tumor-bearing mice 11 days post tumor transplant. Tumor-bearing animals received the indicated ICT treatment on days 3, 6, and 9 post transplant. Representative data is shown. (d) Quantification of percent mLAMA4-specific lysis from independent *in vivo* cytotoxicity assays described above is shown as average ± SEM (n=6 in αCTLA4, n=8 in all other groups). p values calculated using a 2-way ANOVA with multiple comparisons corrected with the Bonferroni method.

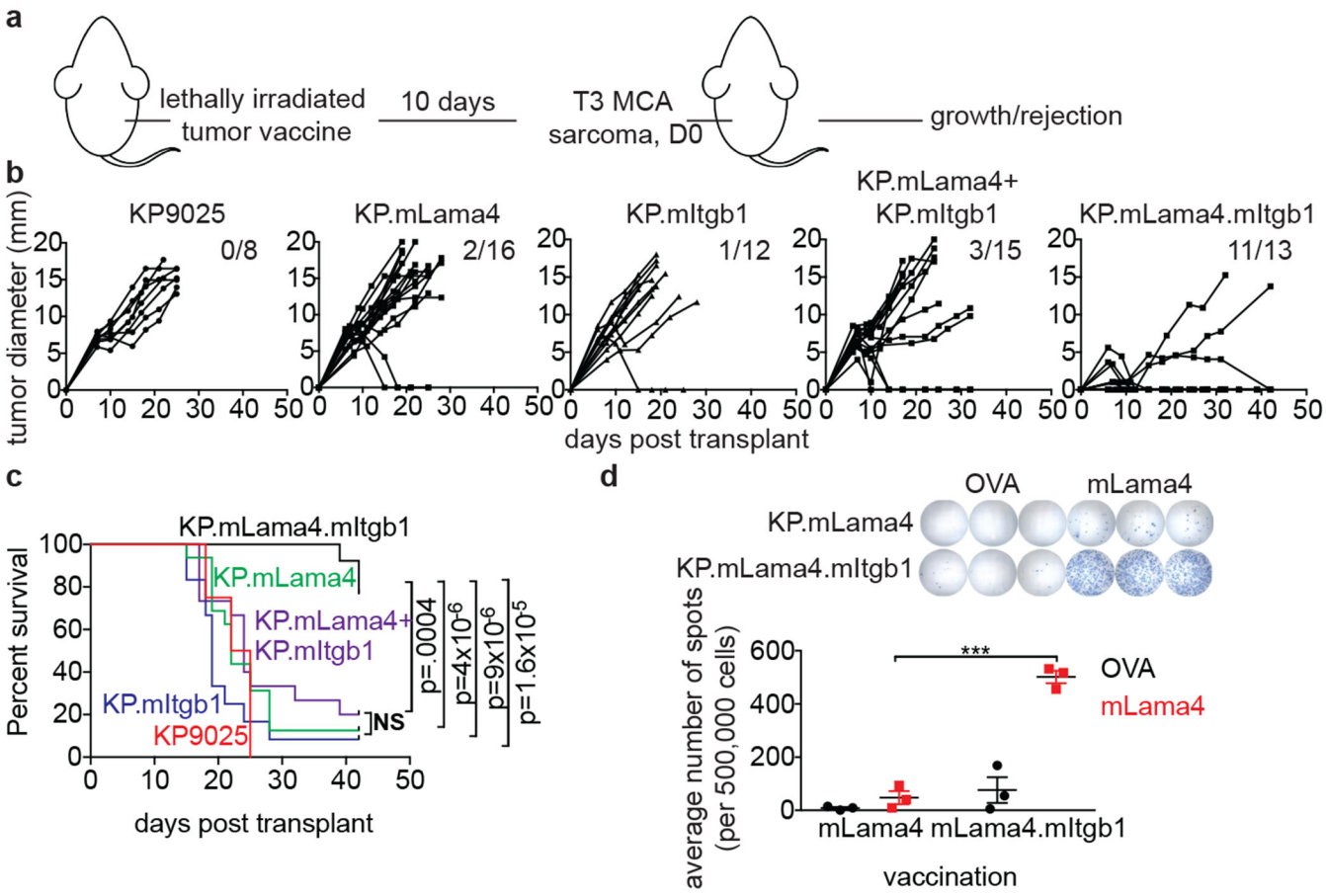

Figure 4: MHC class II neoantigens are required for optimal tumor vaccine efficacy.

(a) Schematic of tumor vaccine strategy. Naïve syngeneic 129S6 mice were vaccinated with $5x10^5$ lethally irradiated KP sarcoma cells expressing the indicated antigens. Ten days following vaccination, animals were injected with $2x10^6$ T3 sarcoma cells on the opposite flank and T3 growth or rejection was monitored. (b) Growth curves of T3 sarcoma cells in vaccinated mice as described above. Data are individual tumor diameters from mice injected in 3 independent experiments (n for each group indicated in figure). (c) Kaplan-Meier curves showing survival of mice described in (b). Indicated p values were calculated using Mantel-Cox tests. (d) ELISPOT analysis of 1 μM peptide-pulsed splenocytes 10 days post-vaccination of naïve mice with irradiated KP.mLAMA4 or KP.mLAMA4.mITGB1 cells as described in (a). Data from three independent experiments is shown as average number of spots ± SEM. ***indicates p=.0002 (unpaired, two sided t test).

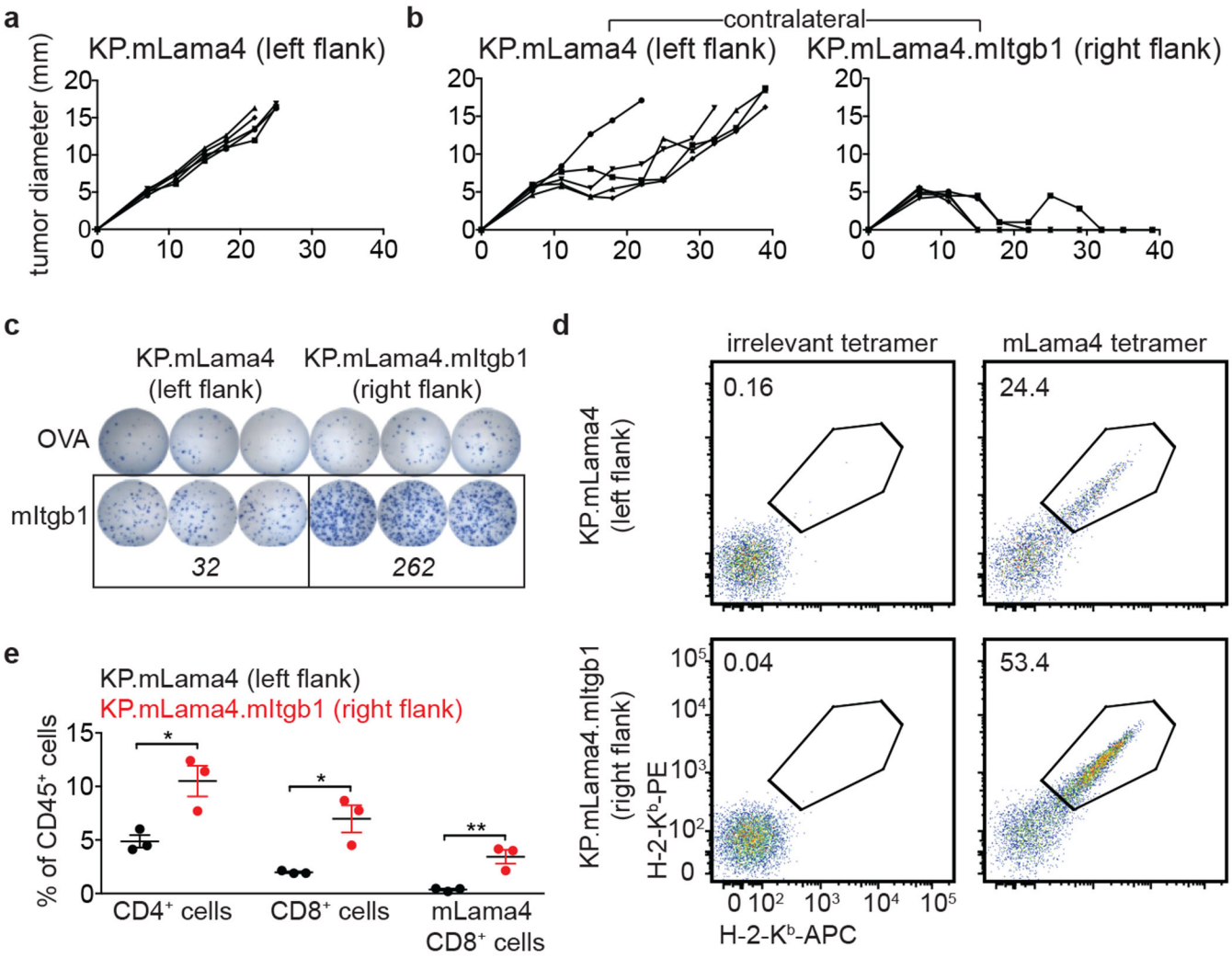

Figure 5: Expression of an MHC-II neoantigen by tumor cells has localized impact on tumor composition.

(a) WT syngeneic 129S4 mice were injected with $1x10^6$ KP.mLAMA4 cells followed by treatment with αPD-1+αCTLA4 on days 3, 6, and 9 post-transplant. Representative data from one of three individual experiments is shown as individual tumor diameters (n=5 per group per experiments) (b) Mice were injected contralaterally with $1x10^6$ KP.mLAMA4 and $1x10^6$ KP.mLAMA4.mITGB1 followed by treatment as described in (a). Representative data from one of three individual experiments is shown as individual tumor diameters (n=5 per group per experiments). (c) Mice were injected as described in (b) and IFNγ ELISPOT analysis of tumor infiltrating $CD4^+$ T cells stimulated with naïve splenocytes pulsed with 2 μg/mL of the indicated peptides was performed 11 days post-transplant. Italicized numbers indicate the average number of spots in mITGB1-stimulated wells from three independent experiments. (d) Tetramer staining of mLAMA4-specific $CD8^+$ TIL 11 days post transplant of mice described in (b). Representative data from one of four independent experiments is shown as percent of mLAMA4-specific cells within the $CD8^+$ T cell population. (e) Quantification of tumor-infiltrating T cells from mice described in (b) 11 days post

transplant. Data is shown as percent of total viable $CD45^+$ cells ± SEM. *indicates p=.02, **indicates p=.009 (unpaired, two sided t tests).